Robotic Compensation of Cerebellar Ataxia

by

Eric D. Smith

S.B. Mechanical Engineering. MIT, 2004

Submitted to the Department of Mechanical Engineering and the
Department of Electrical Engineering and Computer Science
in partial fulfillment of the requirements for the degrees of

Master of Science in Mechanical Engineering

and

Master of Science in Electrical Engineering and Computer Science

at the

MASSACHUSETTS INSTITUTE OF TECHNOLOGY

September 2007

Author .....
Department of Mechanical Engineering and the
Department of Electrical Engineering and Computer Science
August 27, 2007

Certified by .....
Steve G. Massaquoi
Associate Professor, MIT Department of Electrical Engineering and Computer Science
and MIT-Harvard Division of Health Sciences and Technology
Thesis Supervisor

Read by .....
Neville Hogan
Professor of Mechanical Engineering and Brain and Cognitive Sciences
Thesis Reader

Accepted by .....
Arthur C. Smith
Chairman, Department Committee on Graduate Students

Accepted by .....
Lallit Anand
Chairman, Department Committee on Graduate Students

Robotic Compensation of Cerebellar Ataxia

Eric D. Smith

Submitted to the Department of Mechanical Engineering and the
Department of Electrical Engineering and Computer Science
on August 27, 2007, in partial fulfillment of the
requirements for the degrees of
Master of Science in Mechanical Engineering
and
Master of Science in Electrical Engineering and Computer Science

Abstract

The cerebellum is believed to play a role in dynamic compensation in the human motor control system. When it is damaged, subjects make clumsy movements with reduced acceleration, increased overshoot, and swerving in multi-joint movements. These errors, which are referred to clinically as ataxia, are consistent with failing to compensate for the dynamics of the body, especially its inertia during high speed movements. We have developed a robotic system that is capable of dynamically canceling some of the inertial effects in order to reduce the severity of ataxia. This compensator is designed by modeling the closed loop behavior of a subject coupled to a robotic manipulandum. The model is used to solve for the controller needed to produce dynamics in which the inertia of the subject's limb is effectively reduced. The performance of the inertial compensator was tested on both real subjects and a mechanical model designed to reproduce the primary features the subjects' dynamics. The mechanical model provides known and consistent dynamics which facilitates analysis of the compensator performance. The mechanical model confirmed the functionality of the inertial compensator by demonstrating an increase in both the natural frequency and damping ratio of the mechanical model's mass-spring-damper like dynamics. The effect of the inertial compensator on subjects with cerebellar ataxia was measured by their performance on a timed tracing task. The subject with pure ataxia showed a significant improvement in tracing accuracy under inertial compensation, when compared with uncompensated motions. This thesis demonstrates that, in at least some situations, it is possible to mechatronically compensate for the errors associated with cerebellar ataxia by correcting for the dynamics of the limb. This demonstration lends support to the theory that the cerebellum plays a role in dynamics compensation, and it also lays the groundwork for future robotic correction of cerebellar ataxia, a disorder for which there is currently no treatment.

Thesis Supervisor: Steve G. Massaquoi
Title: Associate Professor, MIT Department of Electrical Engineering and Computer Science and MIT-Harvard Division of Health Sciences and Technology

Contents

List of Figures

List of Tables

Chapter 1

Background

The cerebellum plays an important role in human motor control. When it is damaged, subjects retain the ability to move but are impaired in their ability to achieve precise motor goals. Their impairments fall into three broad categories: ataxia (errors in voluntary movements), intention or endpoint tremor, and deficits in motor learning. Many researchers have studied these deficits as a way to gain insight into the role of the cerebellum in motor control. This thesis supports the idea that a unifying characteristic of these deficits is a failure of dynamic compensation [29, 2, 17, 14], and that ataxic errors in particular can be attributed to a failure of the nervous system to compensate for body dynamics. We have tested this hypothesis by developing a system that can reduce the effects of body dynamics and show that this can yield a significant reduction in the movement errors associated with ataxia.

1.1 Anatomy

The cerebellum, or "little brain," is a lobe of the brain located below the occipital lobe of the cerebrum and behind the brainstem. The cerebellum has significant connections to the spinal cord and cerebral cortex by way of the brain stem. These connections carry somatosensory input from the spinal cord, and motor signals from cerebral cortex, among others. The outputs of the cerebellum include projections to motor and premotor areas in the cerebral cortex and brain stem that, in turn, lead to spinal

interneurons and motor neurons. The axons projecting into the cerebellum outnumber the axons leaving the cerebellum by a factor of forty [15].

These connections allow the cerebellum to participate in communication between the motor cortex and spinal cord, but it is not required for signals to be conveyed between the motor cortex and spinal cord. Because of this, the cerebellum is often thought of as a side branch in the motor control system that can tune signals sent between the motor cortex and spinal cord. This is consistent with the observation that damage to the cerebellum leads to altered movements rather than paralysis.

Based on the flow of information through the system, there are two broad functional modes in which the cerebellum can affect motor commands. The cerebellum receives a copy of descending commands from the cortex, which it can filter and add to the motor signal send to spinal cord. In this way the cerebellum can effectively alter the forward signals sent to the spinal system. The cerebellum also receives state information from the spinal cord which it can filter and send back as a motor command to the spinal system. In this way it can contribute to long loop reflexes in the motor system.

The cerebellar cortex has a highly regular anatomy that has been well documented [15]. The cerebellar cortex is composed of many similar cerebellar circuits. A figure of one of these circuits is shown in figure 1-2. Input signals are carried into these circuits on mossy fibers which connect to parallel fibers by way of granule cells. Output signals are carried by deep cerebellar neurons which are driven by mossy fibers and purkinje cells. The synaptic strength between the parallel fibers and purkinje cells can be adjusted by a training signal carried by the climbing fibers. This would potentially allow the cerebellar circuits to act, in a general sense, as a tunable filter system.

1.2 Damage to the cerebellum

There are currently over 15,000 individuals suffering from cerebellar ataxia in the United States [21]. There are many possible causes including stroke, physical trauma, toxic exposure, and a number of inherited disorders that result in progressive degen-

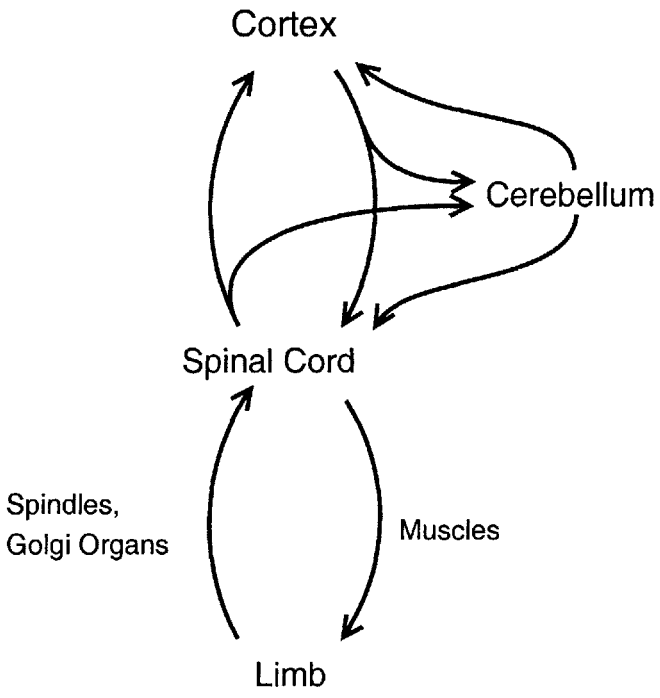

Figure 1-1: Primary paths of information flow in the human motor control system related to the cerebellum.

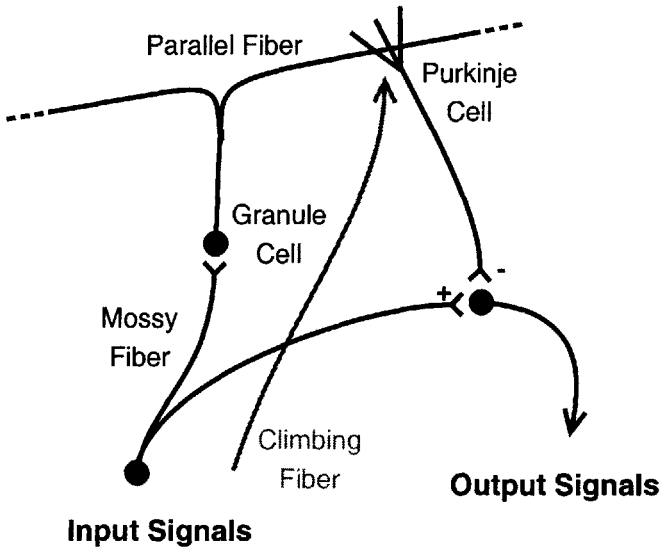

Figure 1-2: The anatomy of the micro-circuit units that make up the cerebellum. These units act as tunable filters.

eration. The type and severity of symptoms are largely determined by the location and extent of the damage rather than the specific cause of the damage [19]. This implies that we may be able to develop a single compensation system that is effective in treating patients with a wide range of afflictions.

1.3 Deficits resulting from cerebellar damage

The three main classes of functional deficits due to cerebellar damage are *ataxia*, deficits in motor learning, and end-point tremor. These deficits impact many forms of movement including gait, speech, and eye and limb movements. Here we will focus on deficits in reaching movements because they are well documented and characterized, and because they can be observed and influenced by a manipulandum.

The term ataxia is often used to loosely describe "uncoordinated" movements. Here we will use the term to refer specifically to the kinematic errors that occur when a patient makes a voluntary movement. For example, in single joint, point to point reaching, ataxic movements tend to have a delayed initiation and delayed peak velocity during the movement[21]. They tend to overshoot their target, and appear to have a lower damping ratio than movements made by healthy subjects. The overshoot becomes larger with faster movement speeds. Adding mass to the limb also exaggerates overshoot [20].

Additional ataxic errors become apparent in multijoint movements. Cross-body ataxic movements tend to be significantly more curved than movements made by healthy subjects [24]. Unlike healthy movements, the movement launch is often not in the direction of the target, and the hand path does not follow a straight line as shown in figure 1-3. This figure, taken from Massaquoi and Hallet [24], shows typical high speed cross-body reaching movements for healthy and cerebellar subjects. More complex movements yield compounding errors that lead to an overall uncoordinated appearance.

Cerebellar damage also leads to deficits in motor learning. Unexpected motor disturbances cause subjects to make movement errors. If a healthy subject repeatedly

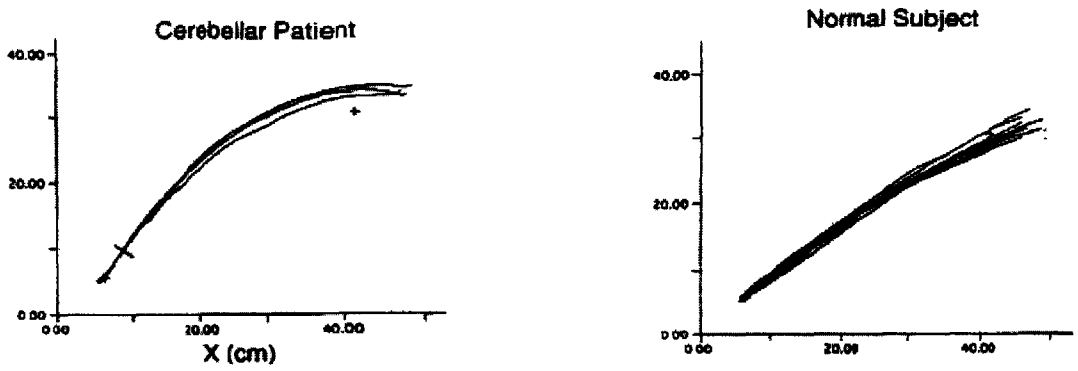

Figure 1-3: Hand paths for cross-body reaching movements for normal and ataxic subjects (from Massaquoi and Hallett 1996 [24]).

experiences a disturbance, then he will slowly learn to compensate for the disturbance and eliminate the movement error. If the disturbance stops occurring, then the subject will initially over-correct in the opposite direction before returning to normal with practice. This form of motor learning is significantly impaired in cerebellar subjects. Cerebellar subjects continue to make movement errors while a disturbance is present and immediately return to normal when it ceases. This type of deficit has been demonstrated in reaching movements in curl fields [27, 23], force steps in postural maintenance [13], and prism adaptation experiments [22].

Another common result of cerebellar damage is endpoint or "intention" tremor. This is an unintentional oscillation that occurs in subjects limbs. It is particularly evident following movements upon target arrival, or when attempting to track a target. The tremor is exaggerated when subjects focus on remaining still or performing precise tasks. This relation to effort prompted use of the term "intention," however, it is more correctly referred to as an "endpoint" or "postural" tremor. The frequency of the tremor is generally between 3 Hz and 5 Hz with more massive body parts oscillating at lower frequencies. Endpoint tremor can occur during movements and may be the cause of undershooting of targets that is occasionally observed in point to point reaching movements. The amplitude of these oscillations can be reduced by coupling additional mass to the limb [10].

1.4 Models of cerebellar function

Over the years, several researchers have combined knowledge of the anatomy of the cerebellum with functional observation of what happens when it is damaged to produce control theoretic models of the function of the cerebellum. One of the most widely known of these models is Kawato's feedback error learning model [17]. In its simplest form, this model proposes a neural network model of the cerebellum that learns to modify feed-forward motor commands to compensate for movement errors. Massaquoi[14] has proposed an alternative known as the Recurrent Integrator Proportional Integral Derivative (RIPID) model. This model proposes that the cerebellum acts essentially as a PID compensator which operates on an error signal between the desired and sensed position of the limb. Because it operates on an error signal it can provide coupled impedance and feed-forward compensation.

Both models place the cerebellum in a signal processing role between low level muscle and spinal reflex systems and the high level motor cortex and parietal lobe systems. The low level systems provide mechanical and reflexive feedback that pull the limb towards the desired location using models similar to the equilibrium point theories proposed by Feldman[5], Bizzi[3], and Hogan [11]. The high level system performs target selection and at least crude path planning, providing desired trajectories to the lower level systems. In both the RIPID and feedback error learning models, the cerebellum acts as a signal processor between the high-level and the low-level systems providing dynamic compensation to improve tracking of the desired trajectory. Because of its feedback control, the RIPID model also appears to account for the role of the cerebellum in postural stabilization and lack thereof (postural tremor) when the cerebellum is damaged.

In the simplest form of feedback error learning, the cerebellum is modeled as a neural network that has the ability to warp a desired trajectory before it is sent to the low-level system. The neural network is trained by an error signal generated from the difference between the desired path and the achieved path. With practice this system is able to learn a feed forward cancellation of plant dynamics. Because sensory

information is only used as a training signal for the cerebellum, this model does not allow for an adaptable long-loop impedance. A block diagram of the simple feedback error learning model is shown in figure 1-4B.

The RIPID model proposes that the signals entering the cerebellum are error signals formed by the difference between desired location and sensed locations. Because it is acting on error signals rather than purely descending commands, the cerebellum can influence both the closed loop impedance of the limb and influence the feed-forward signal sent to it, though these cannot be controlled independently. To date, an algorithm for self-adaptation of the RIPID model has not been proposed. A block diagram of this model is shown in figure 1-4A.

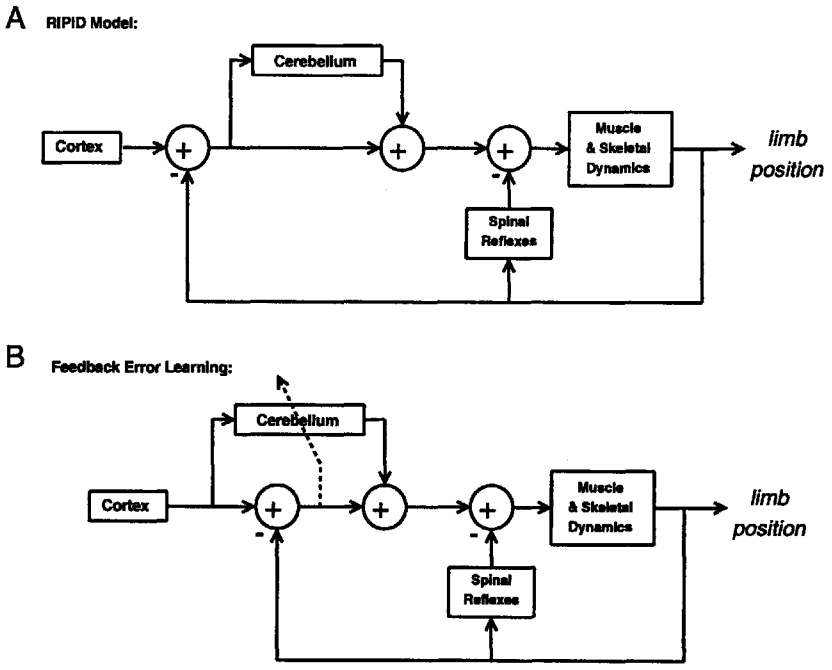

Figure 1-4: Block diagrams depicting the paths of information flow in the RIPID and Feedback Error Learning models.

In both models the motor cortex has direct connection to lower level systems. If the cerebellum is damaged, motor signals are still able to get to the periphery, they just fail to benefit from additional cerebellar filtering. Both models represent the low-level system as a low impedance feedback controller that attempts to track the

descending command. The low impedance of this system results in poor tracking when the added long-loop gain and feed-forward cancellation provided by the cerebellum are not present.

The difference between the RIPID and feedback error learning models lies in the connection to, and implementation of, the part of the model representing the cerebellum. In subjects with cerebellar damage, the functioning of this part of the model is at least partly impaired, and for the purposes of simplicity we will assume it is completely eliminated. In this case, both models have essentially the same structure: a low impedance controller that attempts to guide the plant dynamics along a desired trajectory provided by the high level system. Eliminating the cerebellum component removes the additional dynamic compensation provided by this part of the model. The resulting low impedance, uncompensated model will form the basis of our model of motor control in a subject with cerebellar damage.

1.5 Failure of dynamic compensation

Models, such as RIPID and feedback error learning, in which the cerebellum functions as a dynamic compensator, suggest a unified way of understanding ataxia, tremor and motor learning deficits. These models generally treat the cerebellum as some sort of tunable filter that helps the motor system compensate for movement errors. Disruption of this system prevents adaptive compensation of external dynamics (causing motor learning deficits) as well as adaptive compensation for the internal dynamics of the motor system. These internal dynamics include significant transmission delays and significant mechanical loading associated with the limb. Mismanagement of the transmission delays may result in endpoint tremor, and mismanagement of the limb dynamics may result in ataxic symptoms.

Transmission delays can have a destabilizing effect on feedback systems. These delays cause phase lag in feedback signals which can lead to unstable oscillations if the loop gain is too high. This may be the underlying cause of endpoint tremor. It can take as much as 100ms for a long-loop reflex signal to be transmitted from limb

sensory organs to the cortex and returned to the periphery. If a functional cerebellum is not present to manage loop gains and introduce stabilizing phase lead, then the system may go unstable. Attempting to make precise movements may cause subjects to increase their loop gain, which may explain the exaggerated symptoms under these conditions. Evidence that these tremors are the result of a feedback process involving the limb is provided by the observation that more massive limbs tend to have lower frequency oscillations, and the oscillation frequency can be altered by adding mass to the limb. Models, such as feedback error learning, that place the cerebellum in a purely feed forward role cannot explain the origin of this tremor.

Failure to compensate for limb dynamics is consistent with the kinematic errors observed in ataxia. In high speed planar reaching movements, these dynamics are dominated by inertia. The effects of this inertial loading can be seen with a simple mass-spring-damper model of a single joint movement, as shown in figure 1-5. The inertia of the limb can be modeled as a mass element, with muscles and reflexes represented as a spring between the mass location and desired location. A damper to ground represents energy losses and provides a way for oscillations to be dissipated. A high level system provides a minimum jerk reference trajectory to the displacement source representing desired location.

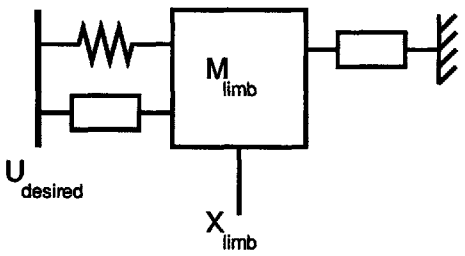

Figure 1-5: A simple lumped parameter model representing limb and muscle dynamics of single joint movements. $U_{desired}$ is a displacement source representing the desired location of the limb set by the CNS, and X_{limb} represents the actual location of the limb mass (M_{limb}). These elements are connected by a spring and damper representing muscle and reflex dynamics. An additional damper to ground represents passive dissipative forces in the limb.

For low speed movements, in which the duration of the movement is significantly longer than the time constant of the mass-spring dynamics, the mass will track the

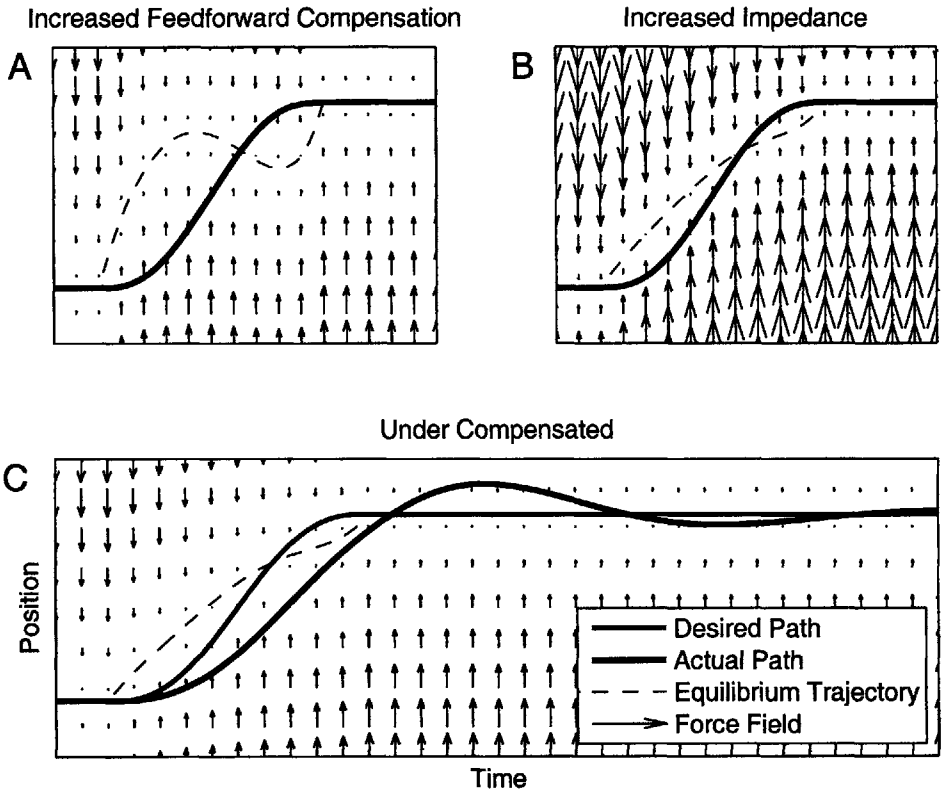

Figure 1-6: A depiction of the muscle forces needed to achieve a given point to point movement. Arrows show the spring force that would be applied by the muscles as a function of position and time, and dashed lines indicate the position of zero force. Accurate movements can be achieved with either feedforward compensation of the limb inertia, or sufficiently high impedance. If neither of these is present then the response is slow and oscillatory.

desired location well and dynamic compensation will be unnecessary. For faster movements, however, dynamic compensation is needed to prevent the inertia of the system from causing poor tracking of the desired trajectory. The cerebellum could provide this dynamic compensation through either warping the feed-forward signal signal before it is sent to the low level system as shown in figure 1-6A, increasing the effective impedance of the low level system through long loop reflexes as shown in figure 1-6B, or some combination of the two.

If neither of these compensation systems is present then the limb will not accurately track the desired trajectory. The resulting errors, shown in figure 1-6C, are consistent with the errors observed when patients with ataxia make high speed single joint movements. The movement has a slower initial buildup of speed, and a delayed peak velocity. It exhibits an overshoot of the target location and an oscillatory response. Increasing the mass makes the overshoot more dramatic which is consistent with Manto's observations [20]. All of these errors are reduced in slower speed movements which is consistent with observations of patients with ataxia, and is a likely explanation for why they choose to make slow movements.

Ataxic errors observed in two-dimensional movements may also be attributed to inertial dynamics. The inertia of the limb is configuration dependent and highly anisotropic. This can be visually represented as an ellipse corresponding to the effective endpoint inertia of the limb as is shown in figure 1-7. The radius of the ellipse represents the degree to which the limb will resist acceleration in any given direction, and the anisotropy is depicted by the ellipse's aspect ratio. A planar two-link arm model such as the one proposed by Flash [7], can be used to predict these inertia ellipses for any arm configuration.

A major portion of the curvature of hand paths seen in ataxic patients documented by Massaquoi and Hallett[24] is consistent with failing to compensate for anisotropies in inertia. The anisotropies make it much easier to accelerate the limb in the direction corresponding to the minor axis of the inertia ellipse than in the direction of the major axis. This means that if muscles apply a force directed at a target, the resulting acceleration will not be in the exact direction of the target, and will instead tend

to favor the direction of minimal inertia. This is consistent with the initial launch angle error observed in curved ataxic movements. The initial acceleration of reaching movements for healthy subjects tend to be in the direction of their target, while the initial acceleration for ataxics tends to veer in the direction of minimal inertia as shown in figure 1-7. This initial launch angle error requires a curved hand path later in the movement in order to reach the target. Coriolis and centripetal effects resulting from changes in these anisotropies may also contribute to the observed swerving.

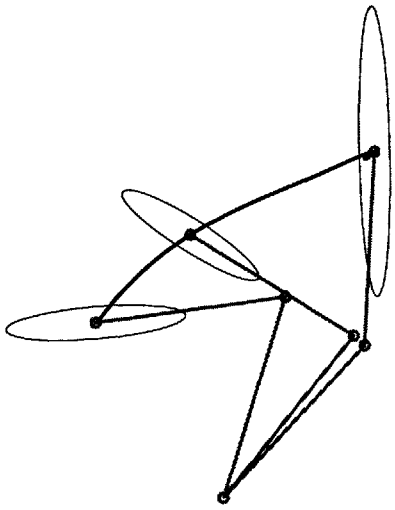

Figure 1-7: Curved hand paths may be the result of anisotropic limb inertia. Here the anisotropy is shown through end-point inertia ellipses for three arm configurations along a curved cross-body movement.

Other researchers have proposed that the cerebellum acts in a more limited dynamic compensation role. For example Bastian proposed that a failure to compensate for interaction torques is the primary deficit observed in ataxia [2]. This can only explain some of the observed symptoms of ataxia. For example, it is incapable of explaining any of the symptoms observed in one-dimensional movements in which interaction torques are not present. Interaction torques are only one part of the inertial dynamics of the limb, and are only able to explain some of the observed symptoms of ataxia. By expanding the model to include a failure to compensate for all internal dynamics of limb and motor system we are able to explain a much broader range of the deficits observed in ataxic patients.

Inertial loading is not the only dynamic force associated with the limb. The damping ratio observed in reaching movements and the impulse response of the limb suggests that in general significant damping is present. These observations are unable to discriminate between damping to ground and damping to the desired location. Only damping to ground will yield kinematic errors. Damping to the desired location will actually improve tracking. Hand trajectories of ataxic movements do not show signs of significant uncompensated viscous loading. This may be because the majority of damping in the system is tied to the desired location. Human muscles and soft tissues have some appreciable viscosity, however, it is not large. The cerebellum may be involved in compensating for some damping to ground, but it appears to be much less significant than the inertial loading.

We have proposed that the errors observed in ataxic movements can be attributed to failure to compensate for disturbances associated with limb dynamics, and in particular, inertial dynamics in planar high speed reaching movements. This theory offers a simple explanation of a single underlying cause for many errors made by subjects with cerebellar damage. It is able to explain slowed movements, overshoot, curved hand paths, and several other characteristics of ataxic movements. The theory is consistent with Babinski's early characterization of cerebellar ataxia as improper adaptation to inertia [1, 21]. Schweighofer's simulations also support it by showing that uncompensated limb dynamics yield hand paths similar to those of ataxic patients when reaching movements are simulated with a low impedance control system [26]. This thesis will directly test if failure to compensate for limb dynamics is the underlying cause of ataxic errors by mechatronically compensating for these dynamics and gauging the impact on ataxic errors.

1.6 Ataxia Compensation

The low impedance, uncompensated model of the motor system not only offers an explanation of the source of ataxic errors, it also allows the errors to be quantitatively predicted. This may make it possible for a robotic system to observe ataxic move-

ments, predict errors, and compensate for them in real time. The errors are believed to be the result of failing to compensate for internal dynamics, which means that if robotic assistance can partially cancel these dynamics, the errors should be reduced. Some dynamics, such as transmission delays cannot be canceled without access to internal signals in the motor system. Other dynamics, such as limb inertia, may be able to be canceled, at least in part, by a robotic system. If this dynamic cancellation does reduce the impairment, then we have both demonstrated that mechatronic treatment is possible, and confirmed the underlying cause of the observed errors.

Other researchers have attempted to mechanically compensate for the deficits associated with cerebellar damage, and have had some limited success. Hewer attempted to treat endpoint tremor by adding mass to the limbs [10]. The treatment was able reduce the frequency and amplitude of tremor, but tended to exaggerate ataxic errors. Dampers have also been used to reduce overshoot and treat endpoint tremor [25]. The drawback to added damping is that it further reduces the subject's ability to make high speed movements, and the additional energy dissipation tends to fatigue patients. We hope to be able to offer significant improvements over these compensation systems by using an active compensator designed around a specific model of the underlying cause of the condition.

Chapter 2

Model of System Dynamics and Compensator Design

Many of the deranged movements observed in cerebellar ataxia appear to be the result of failure to properly compensate for the dynamics of the limb, especially its inertia in high speed horizontal reaching movements. If this failure is the underlying cause, then the errors can be altered by modifying the effective dynamics of the limb. If the inertia of the limb could be reduced, then the effects of not compensating for it would be less severe. Physically reducing the inertia of the limb is not realistic, but using an active control system to make it behave as if it is less massive is an option. This active control system can be implemented in a robotic device that is coupled to the subject, and can sense the kinematics of his movements, and apply forces to modify his effective dynamics. Reducing the effective dynamic loading of the system should yield better tracking of the virtual equilibrium trajectory and reduce the requirement for dynamic compensation from the cerebellum.

For an initial test of this theory we will use an InMotion2 planar robotic manipulandum. This robotic device has been designed so it can be safely coupled to the arm of a patient. Sensors in the device can determine the motion of the arm, and the machine's servos can apply forces to alter the arm dynamics. A real-time computer system is capable of taking these sensor measurements and determining what forces should be applied. In this chapter we will develop an algorithm for this

machine which reduces the effective inertia of a subject's limb when it is coupled to the manipulandum.

Beyond reducing the limb inertia, the compensator must be capable of canceling any additional dynamics that are introduced by coupling the manipulandum to the subject's limb. To accomplish this the controller must be designed around accurate models of the dynamics of the limb, neural controller, manipulandum, and coupling dynamics between them. Here we will initially focus on one-dimensional models and compensator design before generalizing the inertial compensation to the two-dimensional planar case.

2.1 Arm Model

The dynamics of primate limbs during reaching movements has been studied extensively. Hogan has demonstrated that simple linear lumped parameter models are capable of reproducing many of the observed features of one dimensional movements [11]. He has shown that the mass of the limb is driven by muscle and reflex dynamics with largely spring like behavior. The rest lengths of these springs are determined by a displacement source corresponding to a desired location selected by the central nervous system. Reaching movements tend to be well damped. This is modeled by a combination of a viscous damper between the mass and ground, and a viscous damper between the mass and the desired location. A block diagram of this model is shown in figure 2-2.

Combined, these elements form a second order, one degree of freedom system. Hand movements are determined by a combination of particular displacement profile sent in as the reference trajectory, and the natural dynamics of the system. These natural dynamics act as a damped oscillator with a natural frequency given by equation (2.1) and a damping ratio given by equation (2.2).

$$\omega_0 = \sqrt{\frac{k}{m}} \tag{2.1}$$

$$\zeta = \frac{b}{2\sqrt{k\,m}} \tag{2.2}$$

Reducing the effective mass of this system allows the inertia to more closely track the reference trajectory. It also increases both the speed of response, as shown by the increase in natural frequency, and reduces its tendency to oscillate, as shown by the increase in damping ratio. Reduced speed and increased overshoot and oscillations are common features of ataxic movements.

2.2 Machine Model

The manipulandum, shown in figure 2-1, is a planar robot arm whose movements can be controlled by a pair of high torque servo motors. The subject holds a handle which is coupled to the servos by a four-bar linkage. This direct drive configuration minimizes the effects of the drive-train impedance and makes it easily back driven. High quality bearings throughout the system ensure minimal friction. The dynamics of the machine are dominated by the mass of the linkage needed to support the arm.

The servo motors are driven by motor amplifiers that have high-gain current feedback loops. This minimizes the effects of motor dynamics due to back EMF because the motor is essentially driven through a pure current source. The torque out of the motor is directly proportional to this current meaning that the computer can command a nearly perfect torque source. When converted to the linear X-Y coordinates of the handle, these torque sources translate into force sources.

The manipulandum also has encoders on its motors which allow the machine configuration and handle position to be determined. There is also a force transducer on the handle to determine the force that the machine applies to the subject.

These elements combine to produce the model shown in figure 2-2. The model consists of a force source controlled by the computer, a mass element representing

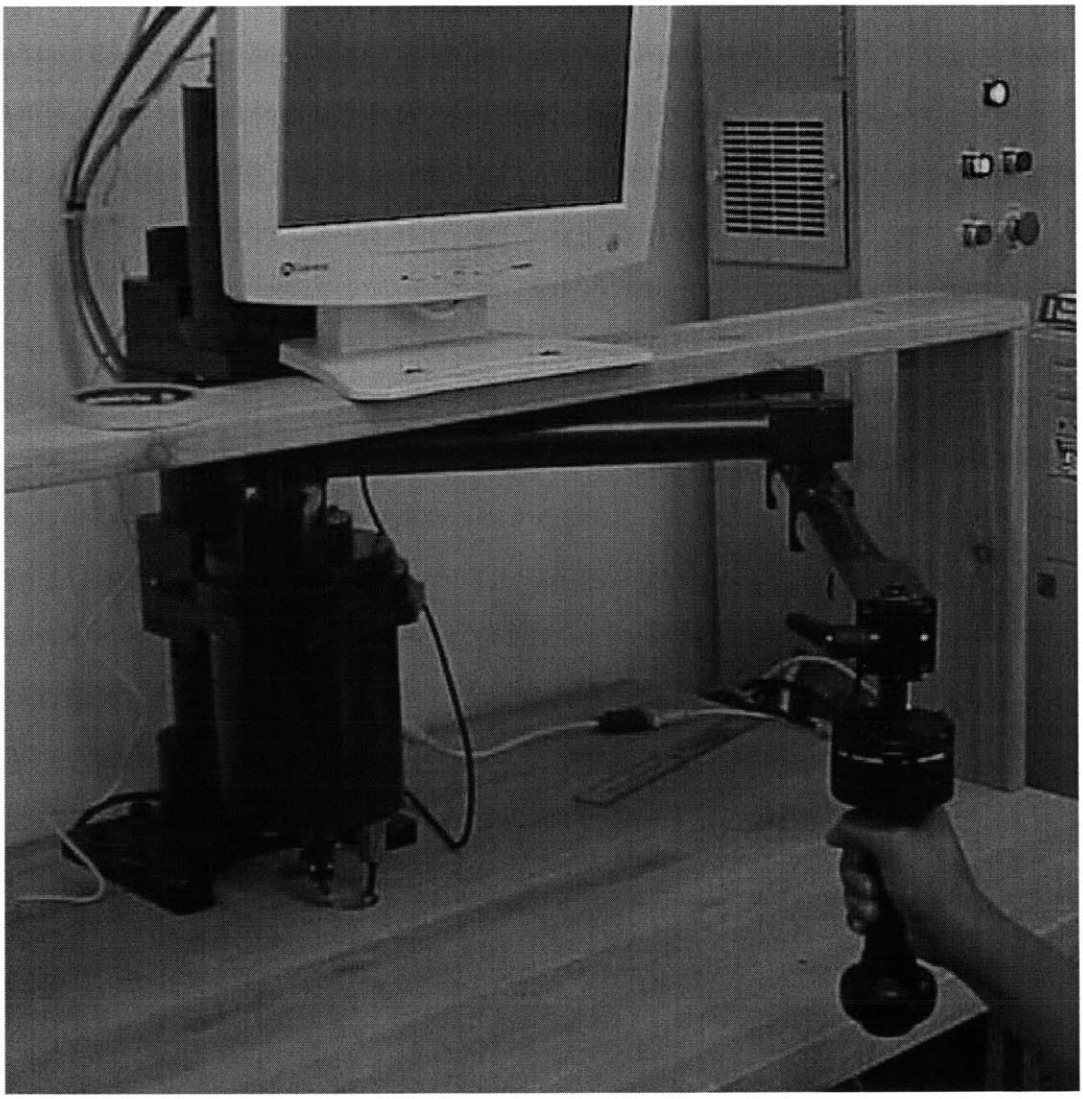

Figure 2-1: An InMotion2 planar robotic manipulandum is used to implement the inertial compensator.

the inertia of the linkage, and a force representing the coupling to the subject. The location of the mass element can be measured by the encoders and the coupling force can be measured through the force transducer.

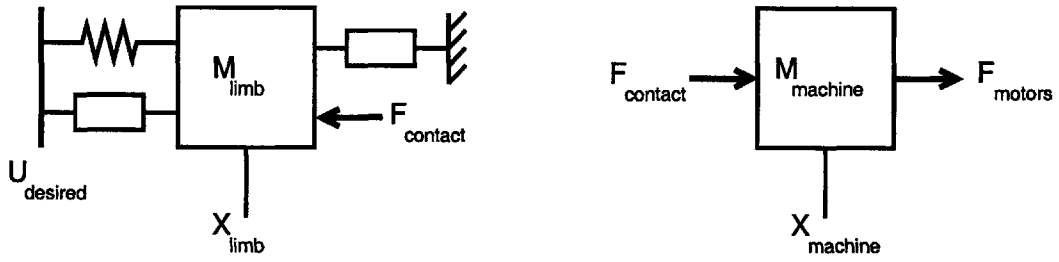

Figure 2-2: One-dimensional lumped parameter models of the dynamics of a human limb and a manipulandum. The manipulandum is represented as a mass element with force sources applied to it representing force output of the motors, and the coupling force applied to the handle. The limb is represented by a mass element with forces applied to it by both a the coupling force, and muscle force represented by the viscoelastic connection to the desired position.

2.3 Coupling Dynamics

Typically, researchers assume that no additional dynamics are introduced by coupling the subject to the machine. This corresponds to modeling the connection between the handle and hand as a rigid coupling. Gillespie and Cutoski's model of haptic interaction is one example of this type of rigid modeling [8].

This approximation works well for many controllers, but inertial compensation is unusually sensitive to errors in the contact model. Inertial compensators are only stable when they are coupled to an inertia equal to or larger than the one they are designed to compensate. If this coupling is not perfectly rigid, then the high frequency impedance seen by the compensator may be smaller than expected. Failing to correct for the effects of non-rigid coupling may destabilize the system.

The potential for destabilization can be seen by considering what happens when the contact is modeled as a spring. At low frequencies, the handle and hand will tend to move in phase with each other, making the rigid approximation reasonable. At higher frequencies, however, the coupling compliance allows the hand and handle

to move out of phase with each other. At these frequencies, the actual effect of the controller will be 180 degrees out of phase from what is predicted by a rigid model. Failing to model the contact impedance can thus lead to unintended effects including the potential for instability.

The nature of hand contact impedance has been studied by human factors researchers interested the development of hand held tools that experience significant vibration [9]. The studies typically consist of a vibrating handle containing force and position sensors that the subject is instructed to hold. These studies show a drop in impedance that begins between 30 Hz and 150 Hz depending on the subject, handle and grip configuration, direction of excitation, and other factors. This change in impedance is consistent with an internal resonance mode in the system.

To capture the effect of an internal mode, a stiff spring and damper are placed between the mass element representing the machine inertia and the mass element representing the limb inertia as shown in figure 2-3. This allows the complete system to exhibit essentially rigid coupling at low frequencies when the machine mass and limb mass oscillate together. At higher frequencies the compliant coupling allows the masses to oscillate out of phase to represent the effect of an internal mode. This mode is only meant to be representative as it is incapable of capturing the many internal modes present in the actual man-machine system.

The dominant compliance is also not necessarily located at the contact boundary between the hand and the handle. For example, the lowest frequency internal mode may occur at the flexibility of the wrist. This would be represented in our model by allowing the mass of the hand to be lumped in with the machine mass and not included in the limb mass. If the lowest frequency mode was in the machine linkage, then some of the machine mass would be lumped in with the limb inertia. For simplicity each of these mass elements will still be referred to by the name of their primary contributor, M_{limb} and $M_{machine}$, but the distinction may not be perfect depending on the primary strain location during the dominant internal mode.

2.4 Combined Model

The models for each component can be combined to give the lumped parameter model of the entire man-machine system shown in figure 2-3. This model is capable of predicting the motion of the limb and manipulandum handle in response to inputs from the subject's desired location and forces applied by the manipulandum. The system has four state variables corresponding to the location and speed of each mass element. The outputs observable by the computer are the location of the machine mass and the contact force at the handle. The contact force may not exactly equal the coupling force transmitted by the internal spring and damper because the dominant internal mode may not occur at the handle contact.

The dynamics of this system can be visualized with the bode plot shown in figure 2-4. Here, the displacement source associated with subject's desired location is held fixed and a range of sinusoidal inputs are applied to the motor force source. The transfer functions plotted use the motor force source as an input and the motor mass location and the coupling force as outputs. Throughout the analysis, the contact stiffness is assumed to be significantly stiffer than the arm stiffness.

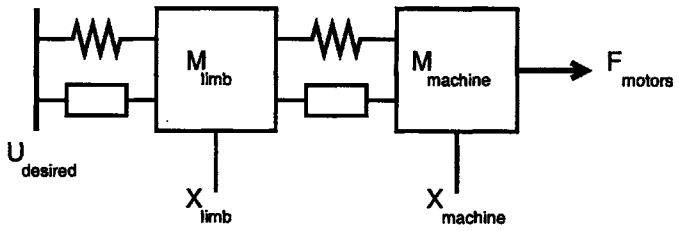

Figure 2-3: Lumped parameter model of a human limb coupled to a manipulandum.

$$\begin{bmatrix} \dot{V}_{machine} \\ \dot{V}_{hand} \\ \dot{X}_{machine} \\ \dot{X}_{hand} \end{bmatrix} = \begin{bmatrix} \frac{-B_{contact}}{M_{machine}} & \frac{B_{contact}}{M_{machine}} & \frac{-K_{contact}}{M_{machine}} & \frac{K_{contact}}{M_{machine}} \\ \frac{B_{contact}}{M_{limb}} & \frac{-(B_{contact}+B_{muscles}+B_{ground})}{M_{limb}} & \frac{K_{contact}}{M_{limb}} & \frac{-(K_{muscles}+K_{contact})}{M_{limb}} \\ 1 & 0 & 0 & 0 \\ 0 & 1 & 0 & 0 \end{bmatrix} \begin{bmatrix} V_{machine} \\ V_{hand} \\ X_{machine} \\ X_{hand} \end{bmatrix}$$

$$+ \begin{bmatrix} \frac{1}{M_{machine}} & 0 & 0 \\ 0 & \frac{K_{muscles}}{M_{limb}} & \frac{B_{muscles}}{M_{limb}} \\ 0 & 0 & 0 \\ 0 & 0 & 0 \end{bmatrix} \begin{bmatrix} F_{motors} \\ U_{desired} \\ \dot{U}_{desired} \end{bmatrix}$$

$$\frac{X_{machine}}{F_{motors}} = \frac{[1] + B_{contact}\, s + K_{contact}}{[1]\ (M_{machine}\, s^2 + B_{contact}\, s + K_{contact}) + (B_{contact}\, s + K_{contact})\ M_{machine}\, s^2} \tag{2.3}$$

$$where : [1] = \left(M_{limb}\, s^2 + (B_{ground} + B_{muscles})\ s + K_{muscles}\right)$$

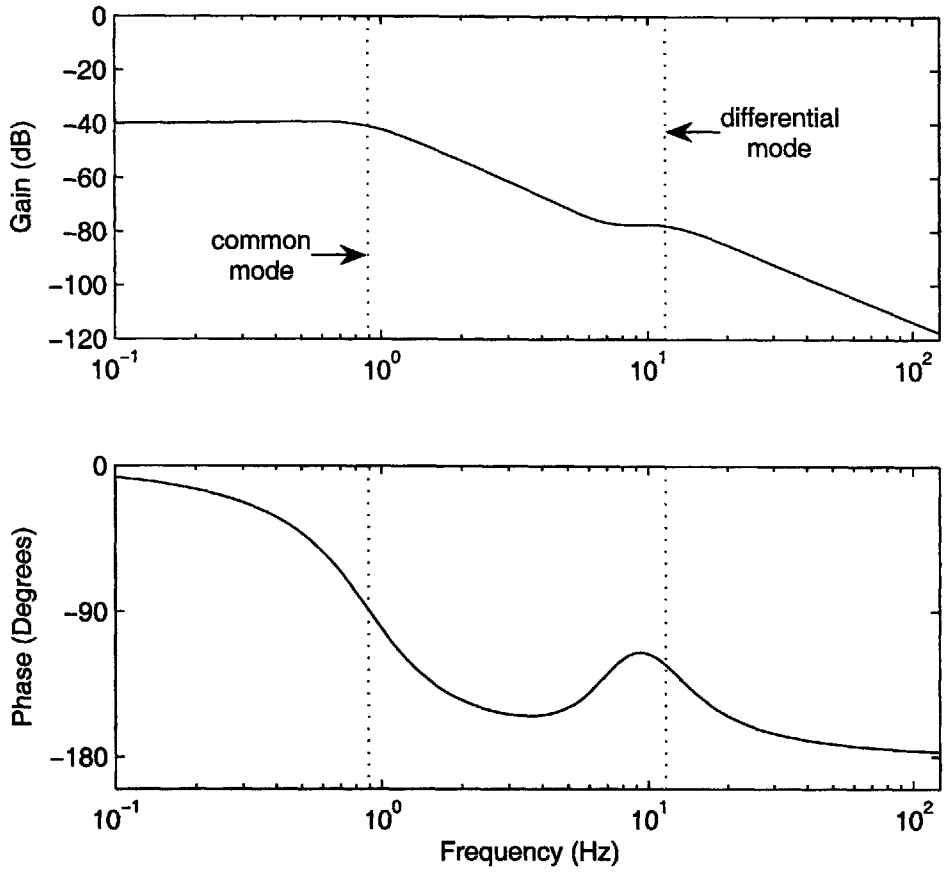

Figure 2-4: Frequency response of the position of the machine mass in response to excitation from the motor force source $\left(\frac{M_{machine}}{F_{motor}}\right)$.

At low frequencies the encoder amplitude is independent of frequency and the amplitude is determined by the stiffness of the muscles. The transducer amplitude is one, or zero on a log scale, because all of the motor force is transmitted through the handle. These levels continue until the drive frequency nears the common resonance

mode at which point both masses oscillate in phase. The frequency of this resonance is determined by the combined mass of the two masses oscillating on the spring associated with the muscles. The amplitude of this resonant mode is determined by the viscous damping associated with the muscles.

At frequencies just above the common resonance mode, the encoder amplitude falls off with -40dB per decade with an equivalent mass of the combined limb and machine mass. The transducer amplitude is determined by a mass divider between the two masses given by equation (2.4). This continues until a zero is reached in the encoder transfer function. The zero is associated with the resonant mode of the limb mass oscillating on the combines stiffness of the muscle and contact springs.

$$FT_{amplitude} = \frac{M_{limb}}{M_{limb} + M_{machine}} \tag{2.4}$$

Above the zero, the encoder amplitude remains flat until the differential resonance mode is reached. This mode occurs at the natural frequency of the two masses oscillating out of phase and coupled by the contact stiffness. The spring displacement is determined by the combined displacement of the two masses, and the ratio of the mass displacements is determined by holding the center of mass of the system fixed. This results in an effective mass for this resonant mode given by equation (2.5). Above this frequency, the encoder amplitude falls with -40dB/decade with an effective mass equivalent to the machine mass, because the remainder of the system has been elastically decoupled at these frequencies. Figure 2-5 depicts the asymptote of amplitude of the encoder transfer function.

$$M_{equivalent} = \frac{M_{limb}\, M_{machine}}{M_{limb} + M_{machine}} \tag{2.5}$$

2.5 Compensator Design

An inertial compensator was designed based on the lumped parameter model of the system. For simplicity, the controller was designed with a single input and single

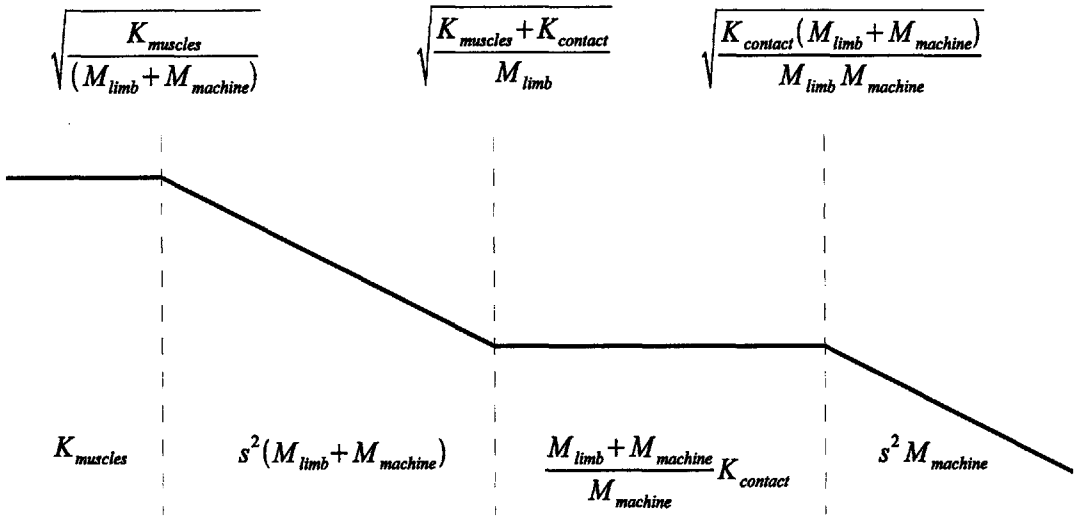

Figure 2-5: Break frequencies and asymptotes of the $\frac{M_{machine}}{F_{motor}}$ transfer function.

output, corresponding to the position of the machine mass and the force source associated with the servos. This controller is represented by the generic controller G. The generic controller can be added to the dynamic equations of the system, eliminating the force source as an undetermined input.

The goal of the compensator is to reduce the effective mass of the limb as viewed from the displacement source representing the CNS. The natural dynamics of the limb in response to this displacement input when the machine is not present are given by the transfer function in equation (2.6). The dynamics when the limb is coupled to the machine is given by equation (2.7). We would like the limb to behave as if the machine were not present and the limbs mass was reduced by $M_{reduction}$. This would result in the desired transfer function given by equation (2.8). The dynamics with the machine present can be solved for the transfer function from desired location to hand position, and this can be equated with the desired dynamics. Solving this equation for G finds the transfer function that must be implemented on the manipulandum in order to reduce the effective limb mass by $M_{reduction}$. This transfer function is given in equation (2.9).

Dynamics without machine:

$$\frac{X_{hand}}{U_{desired}} = \frac{K_{muscles} + B_{muscles}\, s}{M_{limb}\, s^2 + (B_{ground} + B_{muscles})\, s + K_{muscles}} \tag{2.6}$$

Dynamics with machine:

$$X_{hand} = \frac{(B_{muscles}\, s + K_{muscles})\, U_{desired} + (B_{contact}\, s + K_{contact})\, X_{machine}}{M_{limb}\, s^2 + (B_{contact} + B_{muscles} + B_{ground})\, s + K_{contact} + K_{muscles}} \tag{2.7}$$

$$\begin{aligned} where: X_{machine} &= \frac{B_{contact}\, s + K_{contact}}{M_{machine}\, s^2 + B_{contact}\, s + K_{contact} - G} X_{hand} \\ and: F_{motors} &= G\, X_{machine} \end{aligned}$$

Desired dynamics:

$$\frac{X_{hand}}{U_{desired}} = \frac{K_{muscles} + B_{muscles}\, s}{(M_{limb} - M_{reduction})\, s^2 + (B_{ground} + B_{muscles})\, s + K_{muscles}} \tag{2.8}$$

Solving for G:

$$G = \frac{M_{machine}\, M_{reduction}\, s^4 + (M_{machine} + M_{reduction})\, (B_{contact}\, s + K_{contact})\, s^2}{M_{reduction}\, s^2 + B_{contact}\, s + K_{contact}} \tag{2.9}$$

To gain insight into this controller we can simplify it by assuming rigid contact impedance and setting $K_{contact}$ or $B_{contact}$ to infinity. In this case, the controller becomes a negative mass with an amplitude of $M_{machine} + M_{reduction}$, as shown in equation 2.10. When this negative mass is coupled to the positive masses in the system, it will cancel out the machine mass as well as part of the limb mass. If $M_{reduction}$ is greater than M_{limb}, then the total system mass becomes negative and the system becomes unstable. If $M_{reduction}$ is set to zero or less, the controller will not cancel any of the limb mass and may only cancel some of the machine mass. Stable inertial compensation only occurs if $M_{reduction}$ is set between zero and M_{limb}. It should be noted that if $M_{reduction}$ is set in this range, and the limb is not coupled to the machine, then the effective machine mass becomes negative, and the machine goes

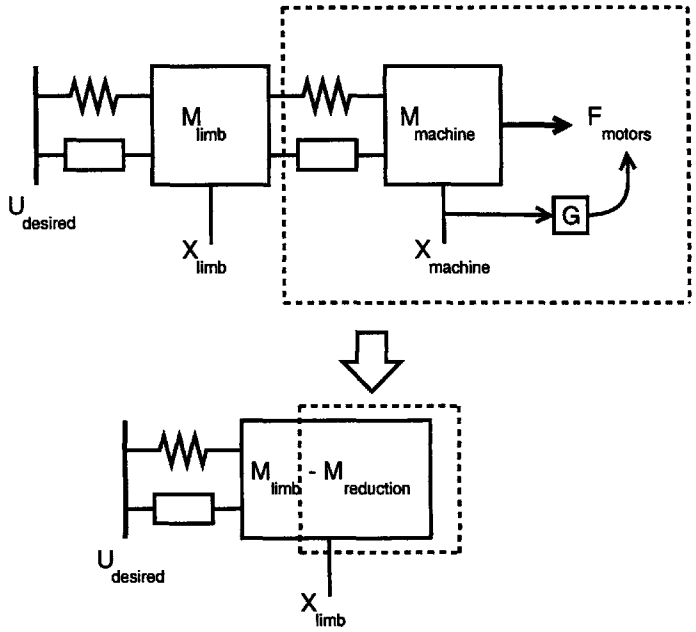

Figure 2-6: The controller, G, is found by solving for the transfer function that will yield the desired dynamics.

unstable. This demonstrates the importance of preventing the subject from releasing the machine when the compensator is active.

if $B_{contact}$ or $K_{contact} = \infty$

$$G = (M_{machine} + M_{reduction})\, s^2 \tag{2.10}$$

$$F_{motors} = (M_{machine} + M_{reduction})\, s^2\, X_{machine} \tag{2.11}$$

If contact compliance is included in the model, then an additional pair of poles and zeros are added to the controller. These essentially act as a lead-lag compensator which reduces the high frequency gain and stabilizes the differential mode. If the system has contact compliance but the rigid controller is used then the differential mode will go unstable. This is because the effective mass of the system above the differential mode is only $M_{machine}$ due to elastic decoupling. The rigid controller will go unstable because of this reduced mass in the same way it will go unstable if the handle is released. This is because the total effective mass of the system has gone negative at these frequencies.

The stabilizing effect of the lead-lag compensator can be seen in a bode plot of

the system. Figure 2-7 shows bode plots for the plant transfer function from motor force to machine mass position, the compensator transfer function from machine mass position to motor force, and the product of these two (or the total loop gain of the system). The contact impedance in the plant has the effect of reducing the total plant impedance at high frequencies. The lead-lag compensator based on the contact impedance model has the effect of dropping the compensator gain at these frequencies. This prevents the total loop gain from becoming significantly larger than unity at these frequencies, and thereby prevents instability. This is a positive feedback system, so loop gains greater than unity can lead to instability if the phase lag is near zero.

Figure 2-7 shows two potential failure modes of the system. If $M_{reduction}$ is set to a value larger than the mass of the limb, then the loop gain of the system between the common and differential modes becomes greater than unity and can cause the common mode to go unstable. Also, if a rigid contact model of the system is used in the compensator design, but the plant contains significant coupling compliance, then the high frequency loop gain becomes greater than unity. This leads to an unstable differential mode.

Errors in the coupling model can lead to instability, but precisely identifying the contact impedance is unrealistic. The impedance is almost certainly nonlinear, anisotropic, and varies with grip and arm configuration. Rather than attempting to identify this quantity, it is possible to directly design the lead-lag compensator from the frequency response of the system. The critical requirement for stability is that the compensator poles occur at or below the differential resonant frequency to prevent the total loop gain from becoming too large. Placing the poles too low does not jeopardize stability, but it reduces the frequency range over which the inertial compensation is effective. The zeros in the compensator are unnecessary for stability, though they can improve the high frequency performance of the inertial compensator. The poles should be placed conservatively low to prevent variation in grip or other disturbances from causing instability. The zeros should be placed conservatively high to guard against instability, especially if other internal resonances are present within

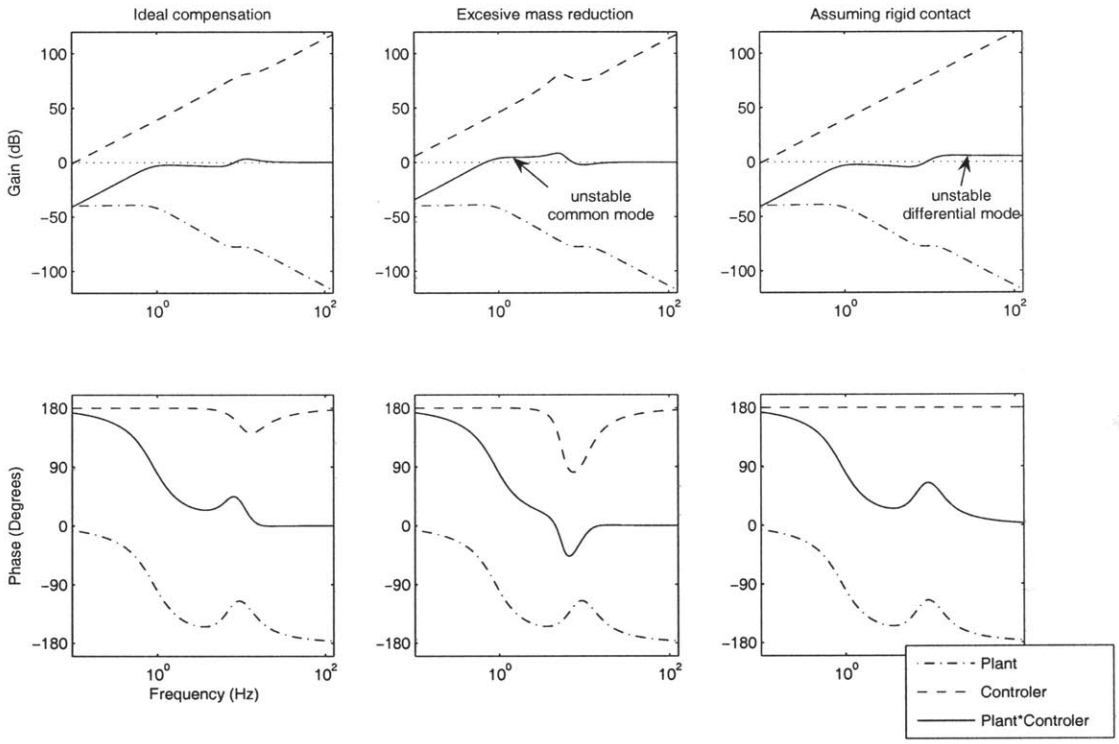

Figure 2-7: Bode plots for the system during ideal compensation, excessive mass reduction, and the assumption of rigid contact. Instability occurs when the total loop gain is greater than unity and the phase lag is near zero.

the bandwidth of the machine. When designing this lead-lag controller, critically damped poles and zeros were used to avoid adding extra oscillatory dynamics.

The overall controller used for inertial compensation is given in equation (2.12). The controller takes the form of a negative mass with a magnitude of $M_{machine}$ plus $M_{reduction}$. A conservative lead-lag compensator represented by $h(s)$ is used to limit the high frequency gain and stabilize the differential mode. An additional non-specific damping term is also added. This term allows the damping ratio and natural frequency of the limb to be adjusted independently.

$$F_{motors} = (M_{machine} + M_{reduction})\, h(s)\, s^2\, X_{machine} - b\, s\, X_{machine} \tag{2.12}$$

Chapter 3

Implementation

The inertial compensator designed in the previous chapter would work well in simulation, but there are a number of considerations that must be addressed before it can be implemented in the real world. First, a system must be implemented which is capable of executing the compensator in real-time. Also, the compensator must have access to an accurate estimate of the current state of the plant. It also needs an accurate estimate of the parameters associated with the plant dynamics. Finally, the effects of any dynamics not explicitly modeled in the compensator design should be minimized.

3.1 Real-Time Implementation

The inertial compensator was implemented on a PC running RTLinux and the InMotion Control software. RTLinux is a hard real-time operating system which is capable of ensuring regular timing and execution of high priority processes. Minimizing jitter in the execution of the control loop is important, because controllers generally assume uniform sample timing. Nonuniform sampling can result in warped estimates of integrals, derivatives, and any other filters that are a function of time.

The compensator system is designed to have two parts: a high speed system which handles all timing critical components, and a slower system which deals with high level control and configuration. The timing critical components are implemented in

C and run as a real-time process. The slower system is implemented in Matlab and communicates with the real-time components via a system of MEX modules.

The bulk of the real-time system consists of Infinite Impulse Response (IIR) discrete time recursive filters. These filters allows for the easy implementation of arbitrary linear controllers specified in the frequency domain. The controllers are designed in the continuous frequency domain and converted into discrete filters using a first-order-hold algorithm. The non-real-time system is capable converting from continuous time controllers, generating filter coefficients, and loading these into the real-time buffers automatically. The ability to load and test new control systems automatically from within Matlab significantly reduced the time required to test and tune the system.

The IIR filters operate on kinematic variables associated with the Cartesian movement of the manipulandum handle. The filters output force commands in the same Cartesian space. Coordinate transforms included in the InMotion control software were used to convert sensor readings into Cartesian endpoint coordinates and generate servo torque commands based on the current machine configuration and the desired endpoint forces.

3.2 Safety Considerations

The nature of inertial compensation leads to controllers that are inherently unstable when the mass for which they are compensating is not present. If the subject releases the handle of the manipulandum while the controller is running, then the handle will exhibit growing, potentially dangerous oscillations. There are several precautions that protect the subject from this potential harm.

First, the compensator is only active when necessary. Upon the completion of the task the compensator is immediately disabled. This eliminates the risk of instability at the time the subject is most likely to release the handle.

Second, the operator keeps careful watch over the subject and has an emergency stop button which can disable the servo amplifiers. The operator watches the actions

of the subject and presses the emergency stop button at the first sign that he may be about to release the handle. The subject is also instructed to inform the operator before releasing the handle. Third, a virtual wall is constructed to protect the subject. This wall consists of a high gain PD controller that only becomes active when the manipulandum handle nears the subject. The boundary at which the controller becomes active also acts as the goal location of the controller, so it has the effect of pushing the handle back to the boundary when ever it attempts to cross the virtual wall. This controller runs in parallel all other controllers and prevents the handle from striking the subject.

Other potential safety options include sensing the presence of the subject's arm and disabling the compensator when it is not present. There are a number of ways this sensing could be done, including use of a grip force sensor, or sensing the vertical force applied to the manipulandum handle by the weight of the arm. These sensing options have not yet been implemented.

3.3 Sensing

For the controller to be effective it needs an accurate estimate of state of the system including the position, velocity and acceleration the manipulandum handle. Accurately sensing all of these quantities over a wide frequency band is difficult with a single type of sensor. The optical encoders used in the manipulandum are good at sensing position and other low frequency kinematics, but quantization and noise make high frequency derivative estimates difficult. Other sensors, such as accelerometers, are good at sensing acceleration and high frequency kinematics, but drift and offset errors make low frequency estimates inaccurate.

These problems are exaggerated by some filters. For example, derivatives and filter zeros amplify high frequency errors from noise and quantizing. This presents a problem when attempting to estimate velocity from an encoder signal. Low pass filters can reduce the high frequency noise, but also introduce lag and eliminate high frequency signals. Integrals and filter poles exaggerate low frequency errors like drift

and offset errors. This presents a problem when attempting to estimate velocity from an accelerometer. High pass filters can be used to make the integrator into a leaky integrator, and reduce the low frequency errors, but may also impair the low frequency signal estimates.

To avoid these problems an integrated multi-sensor approach was used. An accelerometer was added to the manipulandum handle to estimate acceleration. The encoders were used to estimate position, and the encoder and accelerometer signals were combined to generate a velocity estimate. A high pass filtered integrator was used to produce an accurate high frequency velocity estimate. A low pass filtered discrete derivative of the encoder signal was used as an accurate estimate of the low frequency velocity. These filters were designed to be complementary so that their outputs could be added to produce an accurate wide band velocity estimate.

The accelerometer used was an Analog Devices model ADXL203 precision MEMS accelerometer. This model provides two-axis sensing in the $\pm$ 1.7 g range. It has a bandwidth of 2.5kHz, but was limited to 200Hz through a single pole low pass filter prior to sampling. With this filter, it has a typical noise level of 2 mg RMS. The accelerometer was mounted to the end of the manipulandum linkage, coaxial to both the force transducer and manipulandum handle.

The controller form was modified to take advantage of these kinematic variables. For example, the inertial compensator has a transfer function from position to force with two zeros at zero frequency. Rather than taking the second derivative of position, the compensator was modified to make direct use of the acceleration estimate. The viscous terms are also modified to make use of the velocity estimates, and the position terms make use of the encoder readings.

3.4 Machine Dynamics

The inertial compensator is designed around a model of the man-machine dynamics. The closer this model is to the actual dynamics, the better the controller will be at inertial compensation. Any significant dynamics that are not included in the

model either need to be added to the model, or their effects on the system need to be minimized. This section details several dynamics that were easier to physically eliminate than model or compensate for with the control system.

One example is the backlash that results from the small gap between the manipulandum handle and the force transducer. Prior to correction, this dynamic resulted in large force spikes as the machine changed direction and rattled around within this gap. The highly nonlinear nature of this backlash make precise modeling difficult, and the sensing and bandwidth requirements make software compensation impossible. Instead, the handle was modified so that ball bearings could be placed between the handle and the force transducer shaft. This modification eliminated all noticeable play between the handle and the rest of the machine.

Another example is a vibration mode that was present in the table that supports the manipulandum. This mode existed because the table lacked stiff cross braces which are needed to resist horizontal loads. The mode allowed the machine and table to vibrate at around 7 Hz. It prevented proper transmission of force from the machine to the subject near this frequency and introduced undesired oscillations into the dynamics. This was fixed by adding braces to the table to stiffen its connection to ground and add damping. Adding the braces raised the natural frequency to outside the frequency band in which human movements and the inertial compensator are active.

It is also important to constrain any unintentional sources of variation in the system. For example subjects have a tendency to shift their trunks during experiments, and lunge when making reaching movements. These shifts alter the configuration of the arm, and changes its effective endpoint inertia. To minimize this variation, a custom chair was built that constrains the subject's trunk. This chair, shown in figure 3-1, has stiff braces with four degrees of freedom so they can be adjusted to conform to subject's back and constrain the motion of the rib cage. These braces were found to be both comfortable for long duration experiments and effective at constraining trunk movement. A four-point harness was used to hold the subject against the braces and prevent lunging.

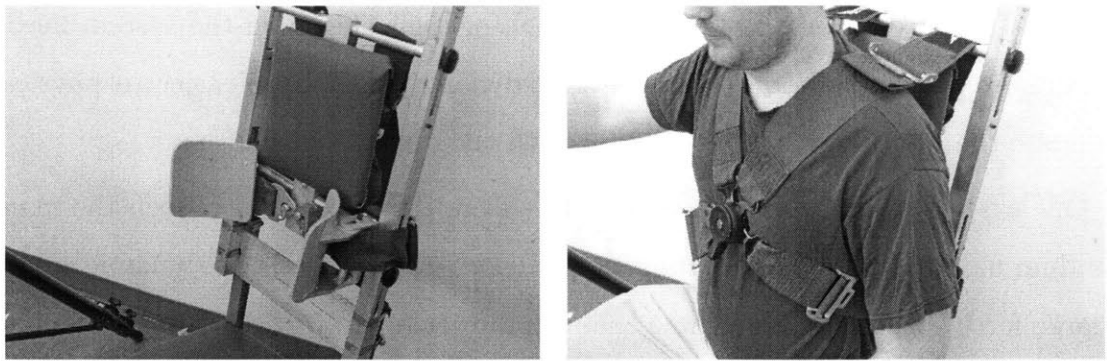

Figure 3-1: Back braces and a four-point harness are used to constrain the subject's rib cage and prevent excessive trunk movement.

The largest discrepancies between the actual dynamics and the model are likely to occur in the model elements that represent the human muscles and motor control. There are a number of aspects of the model that are variable and difficult to sense or predict, such as the descending command sent to the muscles and the muscle and reflex impedance. There are also many delays, nonlinearities and other aspects that are not captured in the simplified lumped model. This is an active area of research so there may be additional dynamics that have not been identified yet.

Fortunately the inertial compensator is not sensitive to these aspects of the model. None of the terms associated with desired location or muscle and reflex dynamics are present in the compensator transfer function. All that is required for inertial compensation is an accurate model of the inertia and a model of how the controller is coupled to it.

The biggest drawback to these model uncertainties is that testing the effectiveness of the inertial compensator is difficult. The descending command to the limb is unknown, so it is difficult to confirm if inertial compensation is making the appropriate changes to the kinematics of the movement.

To eliminate these unknowns, a mechanical model of the human limb and CNS was built. This model has consistent and predictable dynamics. The effects of inertial compensation on this model can be theoretically predicted and physically tested as a way of confirming that the inertial compensator is functioning properly. Testing on this known model allows us to disassociate how effective this controller is at inertial

compensation from how effective inertial compensation is at correcting ataxia.

3.5 Mock Arm Design

To aid in testing, a mechanical model was designed to reproduce the dynamics of our model of the subject's limb and CNS. This mock arm reproduced the limb inertia, the muscle and reflex impedance, and the contact dynamics. The system was able to be coupled to the manipulandum in place of the subject's limb, and had adjustable dynamics so that it could be tuned to match the subject.

For simplicity the mock arm was limited to one degree of freedom. This allowed it to be constructed from a long beam with a rotational bearing at one end and a connection to the manipulandum at the other. Mass, spring and damper elements were connected to the beam, and their effects were modulated by varying the distance between the connection and the pivot point. The length of the beam was long enough to allow a relatively small angular movement to produce a useful endpoint displacement. This minimizes the effects of any nonlinearities associated with a change in angle. When coupled to the mock arm, the manipulandum was programmed to only apply forces in the Y direction, allowing the machine to passively track the curvature of the mock arm endpoint.

The primary mass element consisted of a 2.2 kg block of brass that slid in a track within the mock arm beam. A thumb screw allowed its location along the beam to be easily set. This mass, combined with the moment of inertia of the beam, resulted in an effective endpoint inertia that could be adjusted from approximately .5 kg to 2 kg.

The spring element was implemented through a pair of extension springs with a combined stiffness of approximately 5000 N/m. These springs were sufficiently preloaded so that neither spring went slack throughout the typical range of motion of the mock arm. The springs were connected to the mock arm at a radius that allowed the effective endpoint stiffness to be adjusted in the range of approximately 50 N/m to 500 N/m.

Damping was introduced through a piece of viscoelastic foam that was clamped between the side of the mock arm and a brace connected to the table. The foam was positioned so that it was compressed when the arm rotated, and its location could be adjusted to alter the damping ratio. Preload was added to ensure that the foam always remained in contact with the mock arm. Unfortunately, the short travel of the foam limited the radius at which it could be connected, and prevented the mock arm from achieving the damping ratios typically observed in humans. This low damping resulted in large amplitude oscillations near resonance. The mock arm was given a larger stiffness than observed in human limbs in order to limit the amplitude of these oscillations. These problems could be eliminated by using a different style viscous damper.

The connection between the mock arm and the manipulandum was designed to be compliant to reproduce the differential resonance mode observed in human contact. This was accomplished by placing a flexural hinge between the beam of the mock arm and the bushing mount that coupled it to the manipulandum, as shown in figure 3-2. Flexing of the hinge and twisting of the beam allowed the arm to oscillate out of phase with the manipulandum at high frequencies. Stiffeners could be added to the flexural hinge to adjust the frequency of the differential mode. Viscoelastic foam could be placed between the hinge and the force transducer shaft to adjust the damping ratio of the differential mode. Figure 3-3 shows a picture of the mock arm coupled to the manipulandum.

3.6 System ID

The ability to identify and quantify the plant dynamics is crucial to the compensator design. System identification techniques allowed us to verify that the dynamics of the plant matched the model that the compensator was designed around. These techniques were also useful in verifying that the mock arm dynamics were similar to the dynamics of the real arm. Finally, the techniques allowed us to determine coefficients of the plant dynamics that are needed for the compensator design.

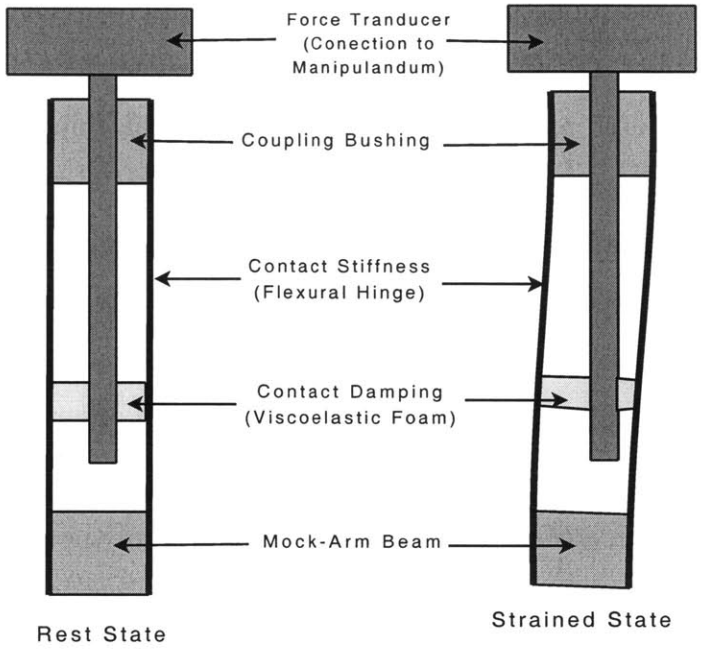

Figure 3-2: Flexural hinges and viscoelastic foam are used to couple the mock-arm Beam to the manipulandum and emulate the contact impedance of the hand.

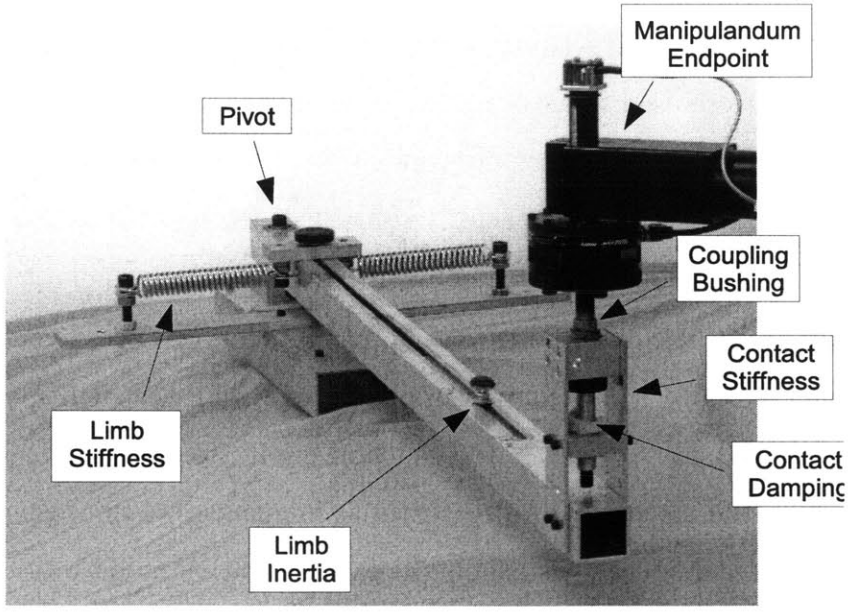

Figure 3-3: Mechanical implementation of the mock arm used to simulate human dynamics and test the compensator performance.

The system ID was done by using the manipulandum to generate experimental bode plots of the plant dynamics. The machine's servos were used to generate sinusoidal driving forces used to excited the system, and the machine's sensors were used to observe these dynamics. The sinusoidal drive was slowly swept over a range of frequencies to excite various modes of the system. The amplitude of the drive was also modulated with frequency. The significant mass of the machine tends to filter out high frequencies, so large drive amplitudes were used at high frequencies. The amplitude was ramped down as frequency was reduced in order to keep the range of motion small, and minimize the effects of configuration-dependent nonlinearities.

The manipulandum's sensors recorded the response of the system. At low frequencies, the encoders were used to measure the movement of the machine mass, and at high frequencies the accelerometer was used. These two signals can be easily combined in the frequency domain to yield a single high bandwidth measure of the mass movement. The force transducer was used to measure the force transmitted by the handle, though this does not necessarily correspond with the coupling force in the lumped model. Other machine states could not be directly observed.

Recordings of the sensor outputs and the signals sent to the servos were chopped into small sections and fit with sin waves. The amplitude and phase of the input and output signals were used to generate the experimental bode plots shown in figure 3.7. The number of samples in each fit window was determined by the period of drive frequency. This ensured that each fit contained a consistent number of cycles and minimized the distortion due to nonlinearities.

The use of swept sinusoidal excitation has some advantages over other excitation modes such as white noise. For example, it allows for visual inspection of excited dynamics. It is easy to watch the machine as it sweeps out frequencies and see which parts of the machine vibrate at various frequencies, even if there are no sensors attached to these modes. This is how the table vibration mode was identified, as well as several others including a vertical vibration mode of the manipulandum handle.

One disadvantages of swept sinusoidal excitation is that it is predictable. If the technique is used at low frequencies on a human subject, it is easy for the subject to

predict and cancel the force applied by the handle. Special attention was taken to get subjects to focus on other activities and ignore the motion of their hand so that they would not alter the descending command to their muscles. Despite these efforts, the low frequency human tests may be quite inaccurate due to unintentional changes in the descending command.

3.7 System ID Results

Figure 3.7 shows experimental bode plots for the manipulandum coupled to a human limb, and the mock arm, and an overlay of these two plots. Both responses show the same basic trend: a flat low frequency response followed by a common mode resonance around 1 hz, followed by a 40dB/decade slope, followed by a differential resonance mode around 12 hz. Both systems also show further internal resonance modes at higher frequencies.

There are several discrepancies between the mock arm and real arm. The resonant modes of the mock arm are significantly less damped than the modes of the real arm. The low frequency asymptotes do not agree, indicating that the mock arm stiffness is unrealistically high, though the measurement in the real arm is likely to be somewhat inaccurate. Also the higher order resonance modes could not be matched.

There are several features in the real systems that can not be reproduced by the lumped model. The order of the model is too low to reproduce the additional high frequency vibration modes seen in the real systems. These modes, along with pure delays in the sensor readings, introduce larger phase lags in the real system than can be produced by the model.

Despite these discrepancies, the model, the real arm, and the mock arm exhibit very similar behavior over a relatively wide frequency band. This implies that the lumped parameter model captures much of the dynamics seen in the real systems and that a compensator designed around it will work well for both the real arm and mock arm. It also implies that testing of the controller on the mock arm will give results that are representative of its performance with the real arm. This allowed us to

carefully test the performance of the compensator without worrying about unknowns and variability in the human motor system.

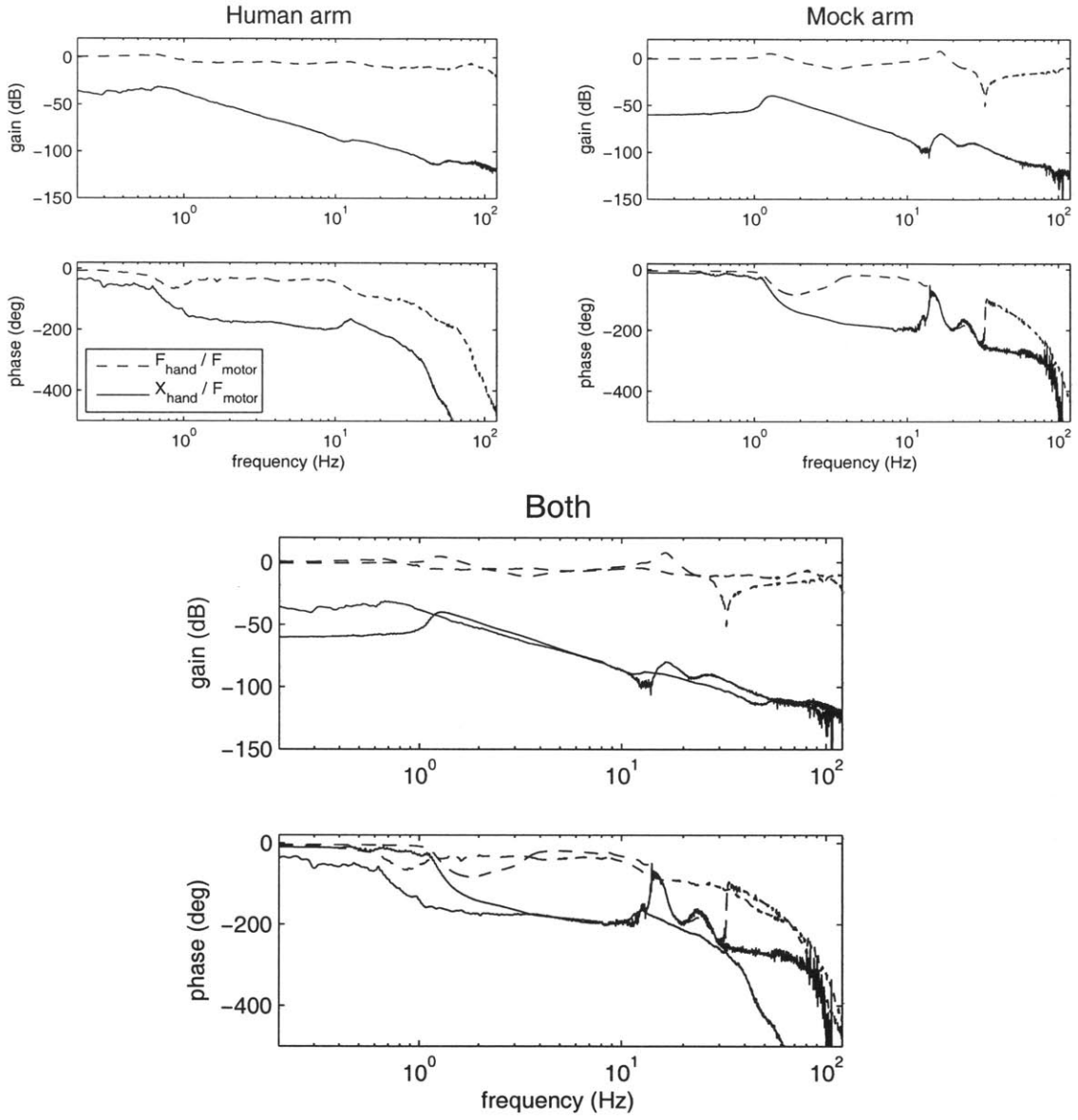

Figure 3-4: Experimentally determined frequency response of the manipulandum when coupled to a human arm and mock arm. The similarity of these dynamics is shown by overlaying these plots.

Chapter 4

Compensator Testing

The performance of the inertial compensator can be easily tested in one dimension using the mock arm. The dynamics of the mock arm are well understood which makes it possible to predict the change in behavior that would result from a reduction in inertia. The actual behavior of the compensated mock arm is easily observed and compared with this predicted behavior. This allowed us to verify that the inertial compensator was functioning properly and map out its performance bounds.

The natural dynamics of the mock arm can be largely captured by a second order mass-spring-damper model. The range of motion of the mock arm was limited to 15 degrees so that a linear model would suffice. In the absence of compensation, the system had a simple damped oscillatory step response. This step response is characterized by its natural frequency and damping ratio.

The second order model predicted that reducing the mass of the mock arm would result in an increase of both the natural frequency and damping ratio of the step response, in accordance with equations (4.1) and (4.2). This can be easily confirmed with the mock arm by adjusting its effective endpoint mass. If the inertial compensator was functioning properly, it would allow these same changes in step response to take place without the mass being physically altered.

$$\omega_0 = \sqrt{\frac{k}{m}} \tag{4.1}$$

$$\zeta = \frac{b}{2\sqrt{k\,m}} \tag{4.2}$$

The compensator has three main parameters that can be varied to alter its performance: the amount of mass that is reduced, the amount of damping that is added, and the frequencies of the poles and zeros associated with compensator gain roll-off. Altering the amount of mass reduction should change both the natural frequency and damping ratio of the step response. Mass reduction levels greater than the total mass of the system should lead to common mode instability. Altering the viscous damping should change the damping ratio of the step response. Altering the roll-off frequencies should affect the high frequency stability of the system. These predictions were tested by observing the step response of the system under inertial compensation.

Unlike a real arm, the goal location of the mock arm is always fixed. To excite the dynamics of the system the mock arm must be displaced off of its rest location. This was accomplished using a high gain PD controller to position the manipulandum and mock arm. The PD controller pulled the mock arm to a constant initial condition away from the rest location of the springs. When the controller released, the springs pulled the mock arm back to its rest location, and the step response of the system was observed.

When the PD controller released the mock arm, the inertial compensator took control. Prior to release, the compensator was allowed to run in the background, filling its filter buffers with sensor inputs and internal states, but not sending its output to the motors. This insured that when it was activated there is not a transient associated with improper initial conditions in the filter buffer. At the moment of release, the signal sent to the motors was switched from the output of the PD controller to the output of the inertial compensator, and the step response of the system was allowed to evolve.

Figure 4-1A shows a typical time course of this process, with time zeroed at the

moment of release. The initial transient that occurs 1.5 seconds prior to release is the PD controller moving the mock arm from its rest location to the goal location of the controller approximately 20 cm away. The mock arm was held here for approximately one second to allow the system to come to rest and ensure consistent initial conditions. At time zero, the PD controller was released, resulting in the observed step response. This process was then repeated with other controller setting to determine the performance of the controller.

The performance of the compensator was determined by varying its control parameters and observing the effects on the step response. Figure 4-1B shows the step response for various values of mass reduction, while damping is held fixed at zero, and the compensator roll-off is held fixed at a conservative value of 8 Hz. As expected, increasing the mass reduction increases the natural frequency of the step response. Increasing the mass reduction also has the unintended effect of reducing the damping ratio of the response. This is presumably due to the inertial compensator not perfectly matching the phase lag of a true negative mass with rigid coupling. If forces produced by the controller are not perfectly in phase with acceleration, then the controller may pump energy into the system yielding the increased oscillation that is observed.

Figure 4-1C shows that, by combining inertial compensation with added viscous damping, the speed of the response can be increased while simultaneously reducing the overshoot. The variation in final resting position of the system is due to coulomb friction in the mechanical system and the relatively weak stiffness of the springs.

The step response with the compensator may not be as fast or well damped as the rising step response of the PD controller, but it is performing a much more difficult task. The PD controller knows its desired location and can bring the system to that location quickly. The compensator is unaware of the goal location because this location determined by the rest length of the springs. The compensator simply ensures that the mock arm can get to its own goal location quickly and in a well damped manner though it is unaware of where this goal location is. This is believed to be what is needed for ataxia compensation: improved tracking of the virtual equilibrium trajectory with out requiring knowledge of the intent of the high level system.

A

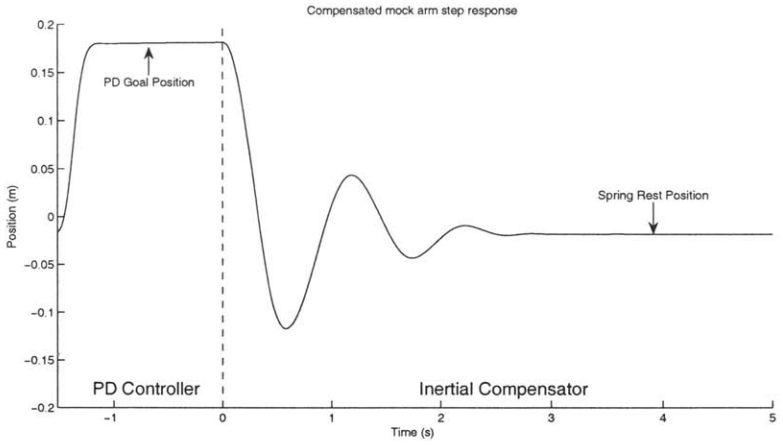

B

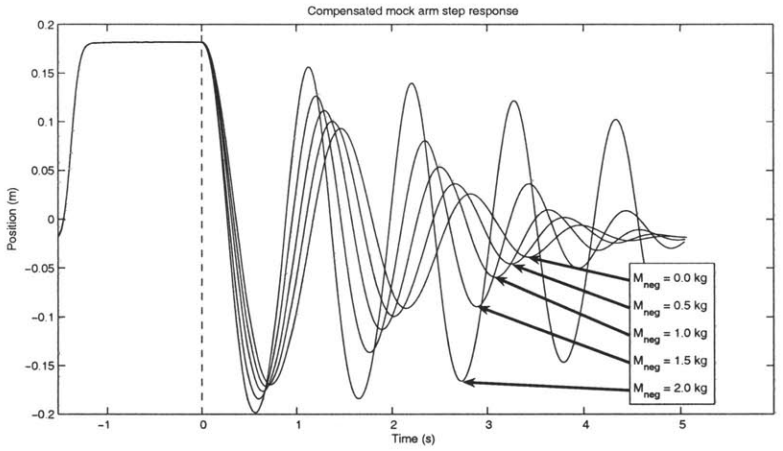

C

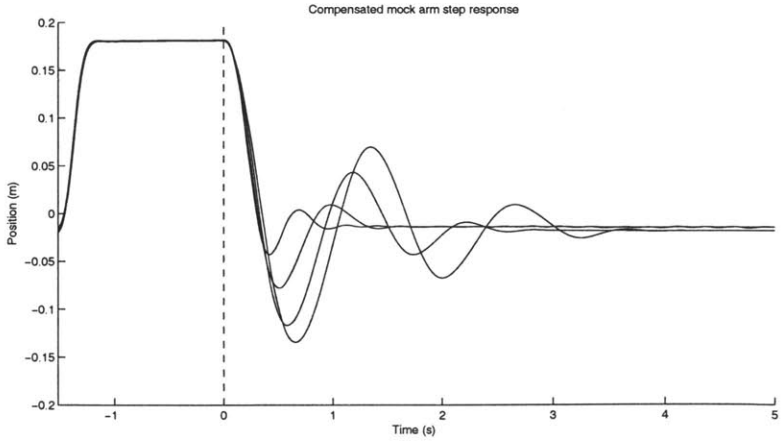

Figure 4-1: Step response of the mock arm under various compensatory settings. Figure 4-1B shows that increasing the mass reduction succeeds in increasing the natural frequency, but has the unintended effect of reducing the damping ratio. Figure 4-1C shows that increasing viscous damping can correct for this.

Additional insight into the performance of the compensator can be gained by observing the power flow through the system, in addition to the kinematics. Figure 4-2 shows the power transferred from the manipulandum handle to the mock arm during the step response. During the step shown in figure 4-2A, the manipulandum motors are set to apply zero force, so that only the passive dynamics of the manipulandum are coupled to the mock arm. The power plot confirms that the passive dynamics of the machine are well modeled as a mass. Initially, the power plot is negative as the mock arm invests energy into accelerating the mass of the machine. At the inflection point in the velocity the power plot passes through zero. Later, as the springs near their rest location, the machine transfers power back into the mock arm as the machine mass is slowed. The added inertia of the machine makes it more difficult for the arm to come to a stop and increases the overshoot.

The inertial compensator can be set to approximate the passive dynamics of the mock arm in isolation by canceling the added mass of the manipulandum. The power plot in which the dynamics of the manipulandum are nullified is shown in figure 4-2B. The RMS power transferred from the machine to the mock arm in the null field has been reduced 65% relative to the RMS power transfer in the passive case. The RMS power transferred in the null field at the handle is 70% less than the RMS power supplied to the motors, showing that the majority of the machine dynamics are canceled out by this compensator. The slight residual forces are uncorrelated with acceleration, indicating that the machine's mass has been effectively neutralized. This forcefield can be used to approximate the situation in which the manipulandum is not coupled to the system. This null field provides a useful control case because it allows the approximate natural dynamics of the system to be observed.

Figure 4-2C shows that the inertial compensator can be turned up to reduce the effective mass of the mock arm. Here, the initial positive power transfer shows that the compensator is pumping energy into the inertia of the the mock arm, boosting the initial acceleration beyond what the springs could naturally produce. Later as the mock arm nears the rest location of the springs, the compensator pulls energy out of the system helping bring the arm inertia to a stop and reducing its overshoot.

By amplifying the acceleration that results from spring and damper forces, the compensator effectively reduces the mass of the system. When the compensator is acting as a negative mass it produces power plots that are roughly the opposite of those produced when the machine is acting as a passive positive mass.

In the step shown in figure 4-2C, the compensator was commanded to reduce the mass of the system by 1.3 kg beyond the mass of the machine. This corresponds to eliminating roughly 70% of the 1.9 kg effective mass of the mock arm. The effect on the system can be judged by the change in natural frequency of the step response. The natural frequency of the system near its rest position was estimated by the difference in time between the peaks of the first and third overshoots. The natural frequency with inertial compensation was 1.89 Hz, just over 80% higher then the 1.04 Hz of the system in the null field. This change in natural frequency represents an effective mass reduction of 70%, the same amount that was commanded.

Power plots are shown for both the power transferred at the handle and the power commanded from the motors. The difference between these plots corresponds to the power absorbed by the manipulandum dynamics. There is a noticeable phase lag between the power commanded from the motors and the power transferred at the handle. This lag is the likely cause of the unintentional oscillations observed in figure 4-1B.

In addition to testing the performance of the compensator, this test setup is also useful in demonstrating the various failure modes of the inertial compensator. If the poles of the compensator are set to too high a frequency, or the zeros are set to too low a frequency, then the differential mode can go unstable. Figure 4-2D shows the power plot and step response of the system with the roll-off set above the differential mode of the system. This results in the high frequency instability shown by the oscillations in the kinematics as well as the power transfer. These plots do not do justice to the violent oscillations that the machine is experiencing during this mode. Nonlinearities in the system presumably keep these oscillations from growing without bound. This underscores the importance of modeling and compensating for internal vibration modes when performing inertial compensation.

The result of excessive mass reduction is demonstrated in figure 4-2E. The compensator causes low frequency instability near the rest length of the springs and results in the limit cycle behavior observed. Increasing the mass reduction results in larger amplitude limit cycles, while increasing the damping limits the amplitude. The system never exhibits nonoscillatory exponential growth as would be predicted by a true negative mass coupled to a positive spring. This is because the negative mass behavior of this system is limited to the control bandwidth of the machine. Above this bandwidth the system will always exhibit passive stable dynamics so it cannot reproduce the behavior of an ideal negative mass.

These tests demonstrate the effectiveness of the inertial compensator and the accuracy of the model on which it is based. The failure modes predicted by the model can be reproduced using the test set up. The parameters are able to increase both the damping ratio and natural frequency of the system. The compensator is able to get the mock arm to its desired location faster and with less overshoot than it would naturally, despite the controller not knowing where this desired location is. This controller looks promising as a way of compensating for ataxia because reduced acceleration and excessive overshoot are the characteristic errors observed in single joint movements.

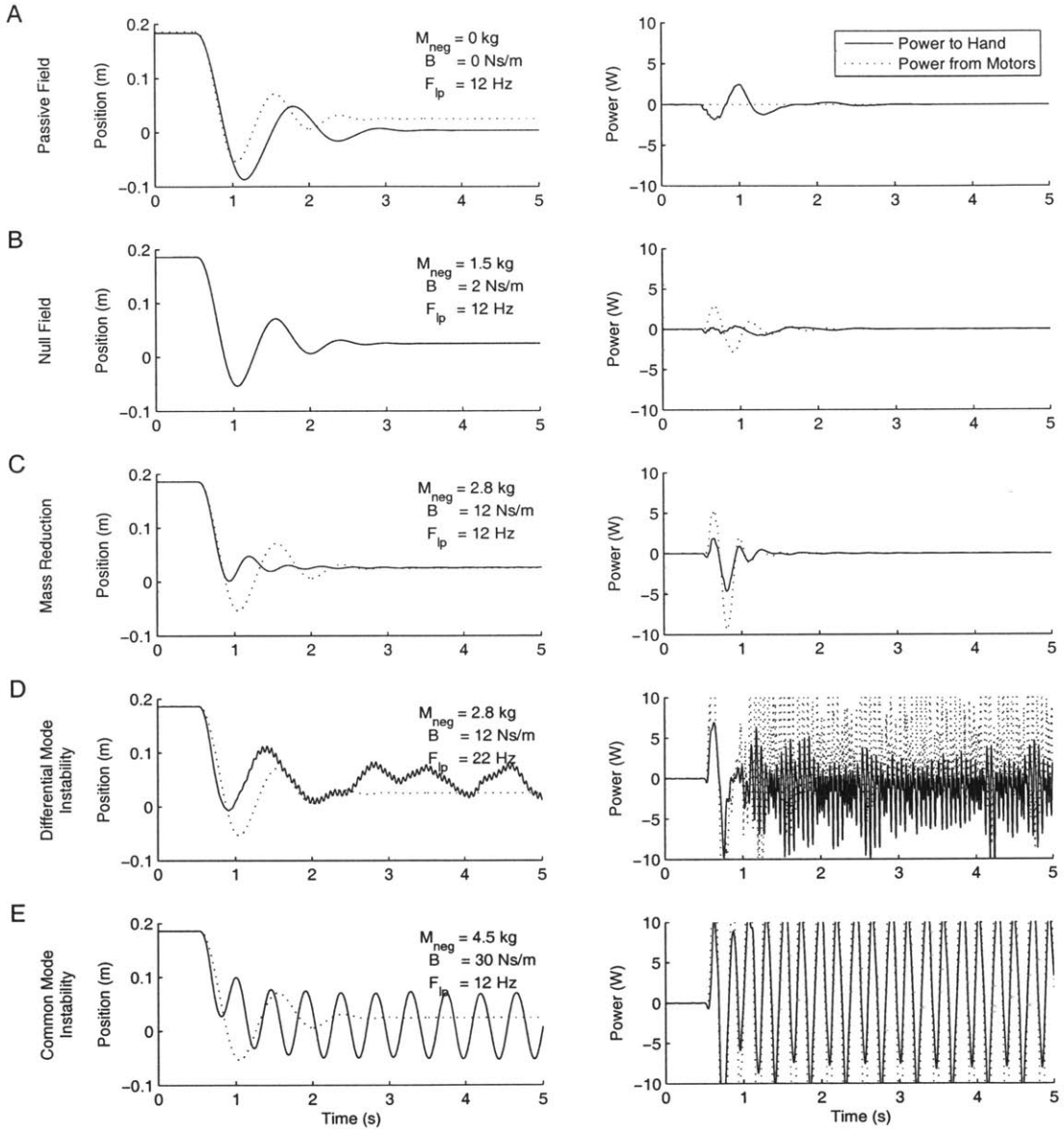

Figure 4-2: Position and power plots of the step response of the mock arm under various compensator settings. The compensator is able to reproduce both null and mass reduction fields as well as both of the predicted failure modes of the system. A dotted trajectory representing the approximate natural step response of the mock arm is included for reference.

Chapter 5

2D Compensator

Many of the deficits observed in ataxia, such as swerving and poor targeting, only occur in multi-joint movements. To affect these errors, the compensator must be generalized in to at least two dimensions. The two-dimensional controller must also work over a larger section of the workspace making configuration-dependent nonlinearities more significant. The added dimensions and added nonlinearities have the potential to make the compensator significantly more complex. This added complexity both makes the derivation more difficult and increases the number of constants that must be identified or tuned. In designing the two-dimensional compensator, we attempted to balance the need for complexity to achieve accurate compensation with the need for simplicity to enable practical implementation.

First we developed a very simple linear two-dimensional compensator that is only locally accurate. Later, it was expanded by including nonlinearities to increase its accuracy over a larger workspace. The two-dimensional controller was derived using a similar process to the design of the one-dimensional controller. The process was further simplified using several shortcuts identified during the one-dimensional derivation. First, rather than directly modeling the contact impedance, we simplified the derivation by assuming rigid contact, and later stabilized the system using a conservative lead-lag controller. Second, the details of the one-dimensional muscle model did not show up in the final one-dimensional compensator solution. This allowed the derivation to be further simplified by replacing all of the muscle dynamics with single

(two-dimensional) force source representing the net force that the muscles apply to the limb.

These simplifications reduced the model on which the compensator was designed to two two-dimensional inertias, representing the effective endpoint inertia of the limb and of the manipulandum. These inertias are rigidly coupled and are acted upon by two two-dimensional force sources representing the effective end-point force of the muscles and the manipulandum motors.

The arm dynamics are represented by equation (5.1) in which F_{muscle} represents the net vector of effective end-point forces applied by the muscles, M_{limb} is the mass matrix representing the effective end-point inertia of the limb, $\ddot{X}_{hand}$ is the vector of accelerations of the hand, and $F_{contact}$ is the vector of contact forces applied to the hand by the machine. Equation (5.2) represents similar dynamics for the movement of the machine mass. Because of the assumption of rigid contact, the acceleration of the machine end-point is equal to the the acceleration of the subject's hand. This allows these equations to be combined and the contact force eliminated from the dynamic equations. The resulting system equation can predict the overall acceleration of the hand and machine as a function of the forces applied by the muscles and motors as given in equation (5.4).

$$F_{muscles} = M_{limb}\,\ddot{X}_{hand} + F_{contact} \tag{5.1}$$

$$F_{contact} = M_{machine}\,\ddot{X}_{machine} - F_{contact} \tag{5.2}$$

$$X_{machine} = X_{hand} \tag{5.3}$$

$$F_{muscles} = (M_{limb} + M_{machine})\,\ddot{X}_{hand} - F_{motors} \tag{5.4}$$

The goal of inertial compensation is to make the limb seem as if it is less massive when it is accelerated by muscle forces. As was done in the one-dimensional case, we can write out the dynamics that we would like to create relating the acceleration of the hand to the forces applied to the muscles as is done in equation (5.5). Here $M_{reduction}$ represents the inertial matrix by which the limb inertia is reduced. These

desired dynamics can be equated to the closed loop dynamics of the system to solve for the motor forces necessary to create the desired dynamics as is done in equation (5.6). The controller needed to create the desired dynamics is given in equation (5.7).

$$
\begin{aligned}
desired: F_{muscles} &= (M_{limb} - M_{reduction})\, \ddot{X}_{hand} && (5.5)\\
= actual: F_{muscles} &= (M_{limb} + M_{machine})\, \ddot{X}_{hand} - F_{motors} && (5.6)\\
gives: F_{motors} &= (M_{machine} + M_{reduction})\, \ddot{X}_{machine} && (5.7)
\end{aligned}
$$

This controller takes a very similar form to one-dimensional controller. The solution shows that the motor force must be a function of the end-point acceleration of the machine, the mass matrix of the machine and the mass reduction matrix. The assumptions of constant coefficients and rigid contact will probably prevent this controller from providing stable and consistent inertia compensation, so these assumptions will be relaxed in the following sections.

5.1 Machine mass

A more detailed model of the machine mass can be derived using Lagrangian Dynamics. This model is capable of predicting how the inertia matrix of the machine mass changes with configuration and determining the additional terms that are introduced by this configuration dependence. The machine's linkage is modeled as four rigid bars. Each bar is parameterized by its moment of inertia, mass, length, and distance along its length to the center of mass as shown in figure 5-1A. Figure 5-1B shows how four of these bars are combined to form the four bar linkage that connects the manipulandum motors to the handle. The generalized coordinates used to represent the state of the system are given by the shoulder and elbow angles of the linkage as shown in figure 5-1C.

The Lagrangian of this system is given by its kinetic energy. This is easily found in terms of the unconstrained coordinates associated with the rotational and trans-

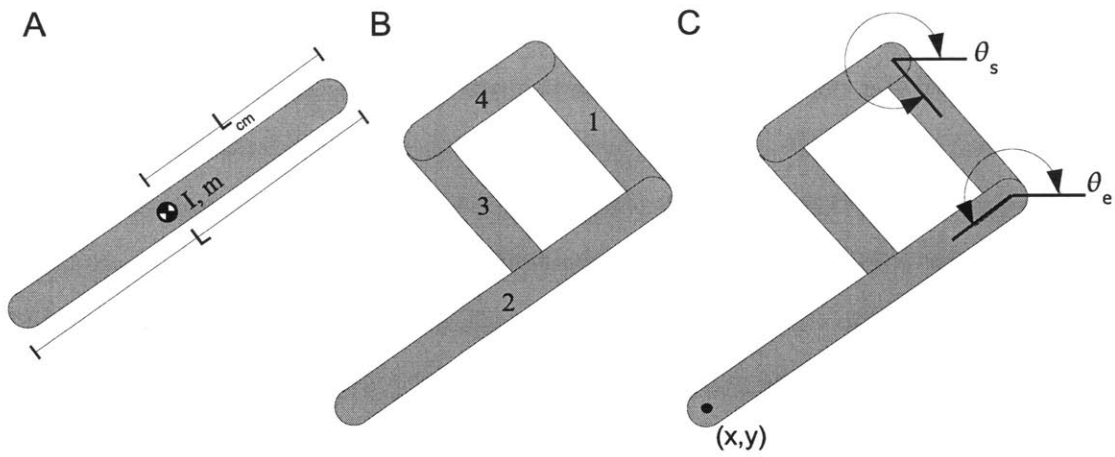

Figure 5-1: The manipulandum is modeled by four rigid bars with moment of inertia I_i and mass m_i. The configuration is determined by two generalized coordinates θ_s and θ_e.

lational velocity of each link about its center of mass as given by equation (5.8). These unconstrained coordinates can be found as a function of the generalized coordinates based on the geometry of the system as given by equations (5.9) though (5.20). The time derivative of these coordinate transforms can then be used to convert the Lagrangian into a function of the generalized coordinate. The Lagrangian can be simplified to the form in equation (5.21) by collecting terms and combining constants. The dynamics then simplify to a form in which there are only two generalized coordinates and three constants representing the inertial dynamics of the linkage.

unconstrained:

$$L = \frac{1}{2} \begin{pmatrix} m_1 \left(\dot{x_1}^2 + \dot{y_1}^2\right) + I_1 \dot{\theta_1}^2 \ldots \\ +m_2 \left(\dot{x_2}^2 + \dot{y_2}^2\right) + I_1 \dot{\theta_2}^2 \ldots \\ +m_3 \left(\dot{x_3}^2 + \dot{y_3}^2\right) + I_1 \dot{\theta_3}^2 \ldots \\ +m_4 \left(\dot{x_4}^2 + \dot{y_4}^2\right) + I_1 \dot{\theta_4}^2 \end{pmatrix} \tag{5.8}$$

unconstrained coordinates in terms of generalized coordinates:

$$x_1 = L_{cm1} \cos(\theta_s) \tag{5.9}$$

$$y_1 = L_{cm1} \sin(\theta_s) \tag{5.10}$$

$$\theta_1 = \theta_s \tag{5.11}$$

$$x_2 = L_1 \cos(\theta_s) + L_{cm2} \cos(\theta_e) \tag{5.12}$$

$$y_2 = L_1 \sin(\theta_s) + L_{cm2} \sin(\theta_e) \tag{5.13}$$

$$\theta_2 = \theta_e \tag{5.14}$$

$$x_3 = L_4 \cos(\theta_e) + L_{cm3} \cos(\theta_s) \tag{5.15}$$

$$y_3 = L_4 \sin(\theta_e) + L_{cm3} \sin(\theta_s) \tag{5.16}$$

$$\theta_3 = \theta_s \tag{5.17}$$

$$x_4 = L_{cm4} \cos(\theta_e) \tag{5.18}$$

$$y_4 = L_{cm4} \sin(\theta_e) \tag{5.19}$$

$$\theta_4 = \theta_e \tag{5.20}$$

Collecting terms and combining constants:

$$L = c_1 {\omega_s}^2 + c_2 \cos(\theta_s - \theta_e)\, \omega_e \omega_s + c_3 {\omega_e}^2 \tag{5.21}$$

$$where: c_1 = \frac{1}{2} m_1 {L_{cm1}}^2 + I_1 + \frac{1}{2} {L_1}^2 m_2 + \frac{1}{2} {L_{cm3}}^2 m_3 \tag{5.22}$$

$$c_2 = m_2 L_1 L_{cm2} + m_3 L_{cm3} L_4 \tag{5.23}$$

$$c_3 = \frac{1}{2} m_2 {L_{cm2}}^2 + I_1 + \frac{1}{2} m_3 {L_4}^2 + \frac{1}{2} m_4 {L_{cm4}}^2 \tag{5.24}$$

The inertia matrix can be directly calculated from the Lagrangian by taking the partial derivative of the Lagrangian with respect to each of the generalized velocities as shown in equation (5.25). This inertia matrix relates the angular acceleration of the generalized coordinates to the application of torques about each of these coordinates. This inertia matrix can be converted into an effective end-point inertia

through a coordinate transform. The coordinate transform from generalized coordinates to end-point coordinates is given in equations (5.26) and (5.27). The Jacobian of this transform is given by equation (5.28). This Jacobian can then be symbolically inverted to give the Jacobian for the transform from end-point coordinates to generalized coordinates. The Jacobian of this inverse transform can then be used to convert the inertia matrix in generalized coordinates to the inertia matrix in end-point coordinates as is done in equation (5.29). The Matlab symbolic tool kit can be used to calculate the equations as well as automatically generate C code that can be used to calculate these values by the real-time controller. Equation (5.31) allow us to calculate the endpoint inertia matrix at any location in the work space as a function of the configuration angles of the linkage.

The inertia matrix in generalized coordinates:

$$M = \begin{bmatrix} \frac{\partial^2 L}{\partial \omega_s \partial \omega_s} & \frac{\partial^2 L}{\partial \omega_e \partial \omega_s} \\ \frac{\partial^2 L}{\partial \omega_s \partial \omega_e} & \frac{\partial^2 L}{\partial \omega_e \partial \omega_e} \end{bmatrix} = \begin{bmatrix} 2\,c_1 & c_2 \cos(\theta_e - \theta_s) \\ c_2 \cos(\theta_e - \theta_s) & 2\,c_3 \end{bmatrix} \tag{5.25}$$

The Jacobian from generalized to end-point coordinates:

$$x = L_1 \cos(\theta_s) + L_2 \cos(\theta_e) \tag{5.26}$$

$$y = L_1 \sin(\theta_s) + L_2 \sin(\theta_e) \tag{5.27}$$

$$J = \begin{bmatrix} \frac{\partial x}{\partial \omega_s} & \frac{\partial x}{\partial \omega_e} \\ \frac{\partial y}{\partial \omega_s} & \frac{\partial y}{\partial \omega_e} \end{bmatrix} \tag{5.28}$$

The effective end point mass:

$$M_{endpoint} = \left(J^{-1}\right)^T M\, J^{-1} \tag{5.29}$$

$$= \begin{bmatrix} M_{ep11} & M_{ep12} \\ M_{ep21} & M_{ep22} \end{bmatrix} \tag{5.30}$$

(5.31)

$$M_{ep11} = \frac{\left(\begin{array}{c} 2\,{L_2}^2 \left(\cos\left(\theta_e\right)\right)^2 c_1 + 2\,{L_1}^2 \left(\cos\left(\theta_s\right)\right)^2 c_3 + \ldots \\ -2\,L_2\,\cos\left(\theta_e\right)\cos\left(\theta_s\right) c_2\,\cos\left(\theta_s+\theta_e\right) L_1 \end{array} \right)}{{L_1}^2 \left(\sin\left(-\theta_s+\theta_e\right)\right)^2 {L_2}^2}$$

$$M_{ep12} = \frac{\left(\begin{array}{c} 2\,{L_2}^2 \cos\left(\theta_e\right)\sin\left(\theta_e\right) c_1 - L_2\,\cos\left(\theta_e\right)\sin\left(\theta_s\right) c_2\,\cos\left(-\theta_s+\theta_e\right) L_1 + \ldots \\ -L_1\,\cos\left(\theta_s\right)\sin\left(\theta_e\right) c_2\,\cos\left(-\theta_s+\theta_e\right) L_2 + 2\,{L_1}^2 \cos\left(\theta_s\right)\sin\left(\theta_s\right) c_3 \end{array} \right)}{{L_1}^2 \left(\sin\left(-\theta_s+\theta_e\right)\right)^2 {L_2}^2}$$

$$M_{ep21} = M_{ep12}$$

$$M_{ep22} = \frac{\left(\begin{array}{c} 2\,{L_2}^2 \left(\sin\left(\theta_e\right)\right)^2 c_1 + 2\,{L_1}^2 \left(\sin\left(\theta_s\right)\right)^2 c_3 + \ldots \\ -2\,L_2\,\sin\left(\theta_e\right)\sin\left(\theta_s\right) c_2\,\cos\left(-\theta_s+\theta_e\right) L_1 \end{array} \right)}{{L_1}^2 \left(\sin\left(-\theta_s+\theta_e\right)\right)^2 {L_2}^2}$$

The configuration-dependent nature of the inertia introduces additional dynamic terms. In rotational coordinates, the terms are commonly referred to as coriolis and centripetal accelerations. These factors can be found from the Lagrangian using the remaining terms in the Lagrange equation that were not already taken into account by the inertia matrix. These velocity dependent terms are given by equations (5.32) and (5.33).

$$\begin{aligned} \tau_s &= \frac{\partial^2 L}{\partial\omega_s\partial\theta_s}\omega_s + \frac{\partial^2 L}{\partial\omega_s\partial\theta_e}\omega_e - \frac{\partial L}{\partial\theta_s} \\ &= -c_2\,\sin\left(\theta_e-\theta_s\right){\omega_e}^2 \end{aligned} \tag{5.32}$$

$$\begin{aligned} \tau_e &= \frac{\partial^2 L}{\partial\omega_e\partial\theta_s}\omega_s + \frac{\partial^2 L}{\partial\omega_e\partial\theta_e}\omega_e - \frac{\partial L}{\partial\theta_e} \\ &= -c_2\,\sin\left(\theta_e-\theta_s\right){\omega_e}^2 \end{aligned} \tag{5.33}$$

A compensator was implemented to cancel out these velocity dependent effects, but it was not included in the final version of the controller. An error in the implementation resulted in tangential forces that were too high and introduced significant curvature to the subject's movements. The source of this error has yet to be determined, so these terms were not included in the version of the controller used during the experiment. This problem should be addressed in future versions of the inertial compensator.

5.2 Mass ID

The Lagrangian analysis shows that there are three constants that characterize the inertial properties of the manipulandum. These three constants must be accurately identified for the compensator to function properly. This identification was accomplished by experimentally mapping out the machine's inertia at one configuration then using this inertia matrix to calculate the constants. These constants can then be used to estimate the inertia matrix at any configuration.

The inertia matrix was mapped out by setting the manipulandum motors to zero force and manually shaking the handle of the machine. The shaking causes the manipulandum to accelerate. The accelerations can be measured by the accelerometer and the force required to cause this acceleration can be measured with the force transducer. Care was taken to shake the manipulandum handle in every direction so that the full inertia ellipse was mapped out. The handle motion was also kept in a relatively small part of the workspace to ensure that the configuration did not change significantly while the data was being collected. To minimize contamination from non-inertial forces, such as friction in the manipulandum, only data points associated with an acceleration greater than 1 m/s/s were included in the inertia fit. The limited bandwidth of the human hand motion prevented significant excitation of the high frequency modes.

The inertia matrix for this configuration was calculated by doing a least squares fit of the accelerometer and force transducer data. Figure 5-2A shows data points

$$
\begin{aligned}
c_1 &= 0.186 \ kg\,m^2 \\
c_2 &= 0.224 \ kg\,m^2 \\
c_3 &= 0.111 \ kg\,m^2
\end{aligned}
$$

Table 5.1: Inertial constants for an early model InMotion2 manipulandum

for force transducer measurements normalized by the magnitude of the corresponding accelerometer reading. These data points are overlaid over an ellipse representing the fit inertia matrix.

The inertia acts as a passive energy storage element. This means that the inertia matrix should have zero curl, making it symmetric. The experimentally determined inertia matrix was averaged with its transpose to force it to be symmetric. Ellipses corresponding to both the full fit matrix and symmetric matrix are shown in figure 5-2A. The relative insignificance of the asymmetric terms can be seen by similarity of these two ellipses.

The symmetric inertia ellipse, along with the average configuration angles of the manipulandum during this fit, can be used to estimate the inertial constants c_1 c_2 c_3 of the manipulandum. Values for these constants for an early model InMotion2 planar manipulandum are given in table 5.1.

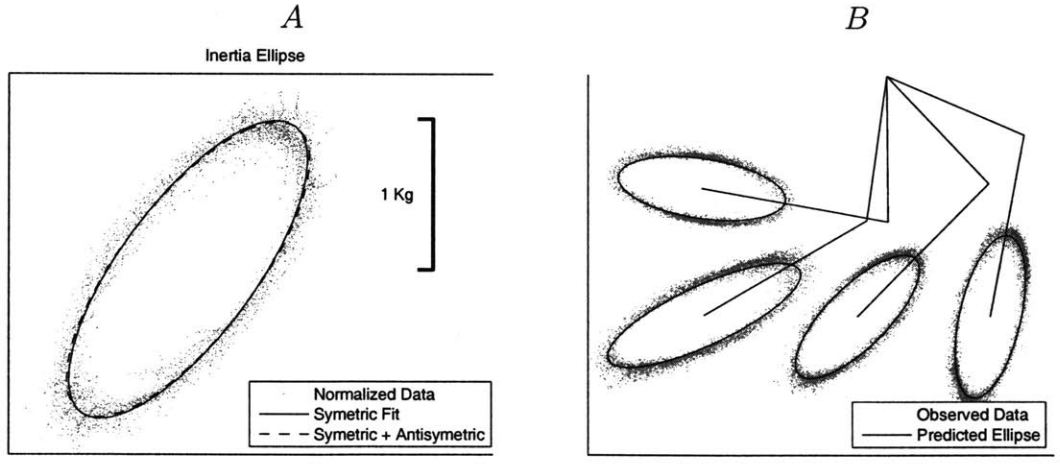

Figure 5-2: Accelerometer and force-transducer data is used to fit an ellipse to the effective endpoint inertia of the manipulandum in figure 5-2A. The inertia model can be confirmed by transforming the ellipse into other areas of the workspace and comparing it with new data at this location as is done in 5-2B

The accuracy of these constants and the inertial model were tested by comparing the model predictions to measured inertia ellipses for other configurations. Figure 5-2B shows measured data for the shaking process of the manipulandum at other locations in the workspace. This data is plotted against the ellipses predicted by the inertial model and the three constants previously identified. The close agreement of the prediction and data confirms the accuracy of the inertia model as well as the identified constants.

5.3 Mass reduction matrix

Part of designing the inertial compensator involves selecting the inertia matrix by which the limb inertia is to be reduced. Ideally, this reduction matrix should be related to the limb inertia so that, as the limb moves about the workspace and changes its effective endpoint mass, the reduction matrix can respond accordingly. This could be implemented using a planar two-link model for the limb similar to the model of the machine mass, and then setting the mass reduction matrix to be a percentage of the estimated limb mass, but this introduces complications.

In practice, this level of detail is difficult to implement. The model requires knowledge of arm kinematics as well as inertial properties, which vary from subject to subject. It introduces four kinematic parameters (the length of links and location of shoulder) and three inertial parameters that must be identified with each new patient. Even with these details, movement of the trunk and shoulder blade can cause additional unsensed disturbances that introduce errors into the model.

In the other extreme, the simplest two-dimensional inertia reduction is an isotropic negative point mass. With this implementation the inertial compensator would reduce the effective endpoint inertia of the limb by equal amounts in all locations in the workspace and equal amounts in all directions. This scheme is easily implemented and requires only a single parameter to be tuned for each subject. However, its performance is quite poor due to the large anisotropies in limb endpoint inertia. The system becomes unstable in the direction of the minor axis of the limb inertia before

a significant percentage of major axis inertia is reduced. The isotropic design is too restrictive to provide useful performance.

A design with an intermediate level of complexity is an anisotropic constant coefficient mass reduction matrix. This solution can be tuned to match the anisotropies of the limb in one part of the workspace, but lacks the configuration dependence of the full two-link model. If the limb does not move far from the tuned location, then its inertia matrix will not change significantly and the compensator will continue to function well. An attempt was made to minimize changes in the inertia matrix by limiting the workspace to a relatively small rectangular area approximately 25cm wide and 20 cm deep located in front of the subject.

The anisotropic constant coefficient design has three parameters that must be tuned, the magnitude, orientation, and aspect ratio of the mass reduction ellipse. These parameters are tuned to match the limb inertia when it is in the center of work space. In practice, only the magnitude of the ellipse must be adjusted from subject to subject.

The orientation of the mass reduction ellipse is determined by the orientation the the subject's limb inertia ellipse, which is primarily a function of arm configuration. The arm configuration at the center of the workspace is held fixed for each subject by adjusting seating location. The seating location is adjusted so that the segments of the subject's arm forms an approximate 90 degree angle, and each segment is 45 degrees from straight ahead. At this configuration, the eigenvectors of the limb inertia are at 45 degrees from straight ahead, along the fore arm segment, and perpendicular to it. The eigenvectors of the mass reduction ellipse are set to match these, and don't need to be adjusted because all subjects are positioned in this configuration at the center of the workspace.

The aspect ratio of the limb inertia ellipse is determined by the mass distribution of the arm. This does vary from subject to subject, but the variability was assumed to be small relative to the variability in the magnitude of the inertia ellipse. In the future, this assumption could be eliminated by identifying inertial constants for each subject. In the absence of such information, the aspect ratio of the reduction ellipse

was tuned by hand by a skilled operator. This was done by shaking the machine along the direction of each of the limb inertia eigenvectors, and tuning the constants such that the effort required to accelerate the limb in each direction was matched.

The magnitude of the mass reduction ellipse must be tuned from subject to subject. This is because overall limb mass varies from subject to subject. If the reduction ellipse is too small for a given limb mass, then the compensator will have a minimal impact on the limb dynamics. If it is too large, then it will cause instability. The magnitude was tuned to each subject by finding the maximum value of reduction that did not introduce limit cycles or other oscillatory behavior into the subject's motion.

The fixed anisotropic design works well over much of the limited workspace of the task, but near the extremes, mismatch between the reduction ellipse and the limb inertia becomes significant. To prevent instability from occurring at these locations, the overall magnitude of the reduction ellipse must be limited. Future versions of the inertial compensator could achieve higher levels of performance by using a configuration dependent mass reduction that is tuned to each subject.

5.4 2D contact impedance

The one-dimensional controller demonstrated that instability would occur if a rigid model was assumed when internal vibration modes were present. The same is true for the two-dimensional controller, however, identifying and modeling the internal modes is much more difficult. The modes are a function of many parameters including the direction of excitation and the configuration of the linkage. Even unsensed states such as the subject's grip force can impact the vibration modes of the limb-machine system.

Rather than attempting to catalog and model the behavior of these modes we borrowed a trick from the one-dimensional compensator. For stability, all that is required is that the gain of the compensator roll-off at a frequency below the lowest internal mode. This means that rather than identifying all of the modes, we can place an isotropic conservative lead-lag compensator on the whole controller. The

compensator may be very conservative for some directions and in some parts of the workspace, but it will be sufficient to stabilize the system, and only introduces two parameters that must be tuned to stabilize the system.

5.5 Viscous Damping

The one-dimensional compensator also demonstrated that inaccuracies in the compensation system could cause the system to become oscillatory. This was corrected by the addition of a viscous damper in parallel with the inertial compensator. A two-dimensional damper is needed to prevent unintended oscillation in the two-dimensional compensator. This damper was designed to include two terms. The first term is a damping matrix that is proportional to the negative mass matrix of the system, or the sum of the machine mass estimate and the mass reduction matrix. This term was selected because the one-dimensional testing showed that larger mass reductions lead to smaller damping ratios and required greater damping. An additional isotropic damping term gives further control over damping in the system.

5.6 Complete compensator

The complete two-dimensional compensator takes a form very similar to the one-dimensional compensator. The compensator is made of a negative mass term determined by a mass reduction matrix and the machine mass estimate as given by equation (5.34). It contains viscous damping terms given by equation (5.35) which can be tuned to improve the damping ratio of the system. It also has an isotropic lead-lag compensator used to stabilize the internal modes of the system given by equation (5.36). The complete compensator is given by equation (5.37). The compensator can be converted into a null field by setting the mass reduction matrix (Mr) to zero and eliminating the damping.

$$M_{negative} = [M_{endpoint}(\theta) + M_{reduction}] \tag{5.34}$$

$$B = b_{isotropic} \begin{bmatrix} 1 & 0 \\ 0 & 1 \end{bmatrix} + b_{mass} [M_{negative}] \tag{5.35}$$

$$H(s) = \frac{\left(\frac{s}{Z}+1\right)^2}{\left(\frac{s}{P}+1\right)^2} \tag{5.36}$$

$$F_{motor} = [M_{negative}] H(s) \ddot{X} - [B] \dot{X} \tag{5.37}$$

5.7 2D Verification

The performance of the two-dimensional inertial compensator was verified by having a subject hold onto the manipulandum and make point-to-point reaching movements. The kinematics of the movements were recorded, along with the forces that the machine applied to the hand. The compensator performance was verified by checking that the forces applied were consistent with inertial compensation under the observed kinematics.

The movement shown in figure 5-3 consists of four point-to-point reaching movements that form a counter clockwise rectangle. The movements were made with in three forcefields: the passive field in which the motors supply no power, a null field in which the controller minimizes the effects of the manipulandum dynamics, and an inertial compensation field in which the controller attempts to reduce the effective mass of the limb. Care was taken to ensure that the hand paths and velocity profiles of these movements were very similar so that the force outputs can be directly compared.

When humans produce point-to-point reaching movements they tend to be relatively straight in endpoint coordinates and have a smooth bell-shaped velocity profile. This results in a biphasic acceleration profile that is primarily along the path of the movement. When coupled to the passive mass of the machine, this results in a bipha-

sic power plot for each movement segments as expected. This plot is shown in figure 5-3. Because the machine is acting as a positive mass, it initially absorbs energy during the launch phase of each movement as indicated by the negative power transfer, and then delivers this energy back to the hand during the braking phase.

Power plots of the movements in the null field have a different shape. The power levels are always negative, or dissipative. The plots are dominated by a single bell shaped curve with almost no sign of a biphasic component. This indicates that the inertial behavior of the machine has been almost completely canceled, and replaced by a small viscous damper. The plot of the power transferred from the motors into the machine mirrors the power plot in the passive field. This shows that the controller is accurately predicting and canceling the inertial dynamics of the manipulandum.

Ideal power plots in the mass reduction field would have a similar biphasic form to the passive plots, but would have the opposite sign. This form is clearly visible in the vertical (second and fourth) movement segments. By comparing the peaks in tangential force to the peaks in tangential acceleration, the mass reduction effect of the controller can be estimated to be just over .6 kg, nearly identical to the commanded level of .64 kg, and roughly 40% of the limb inertia in this direction. The phase lag, discussed in chapter 4, between motor power and handle power plots is also visible in these segments. The lag causes power input during the launch phase to be extended into the peak velocity phase at mid-movement. This causes the controller to put more energy into the limb during the launch phase than it pulls back out during the braking phase. This added energy may increase overshoot. This problem could be corrected through additional damping.

The horizontal (first and third) movement segments show further deformation of the ideal biphasic power plot. The plots show an unintended negative power transfer early in the launch phase followed by a delayed peak input power. The braking assist is also significantly diminished. These are indications that, though the inertial compensator is effective in some parts for the workspace, there is still room for significant improvement in its performance.

Power plots are only capable of representing forces applied in the direction of

motion. Power is the dot product of the force and velocity vectors, so all information about forces perpendicular to the motion is lost. The perpendicular forces can be viewed using the quiver plots in figure 5-3. These shows the hand path taken by the subject with arrows overlaid representing the force applied to the hand by the manipulandum handle at various positions along this path.

Quiver plots in the passive field show forces that are largely aligned with the hand path because this is the direction of greatest acceleration. These forces oppose the motion in the first half of each segment and are in the direction of motion in the second half as was shown in the power plots. The quiver plot in the null field shows forces that also primarily aligned with the hand path, but they always oppose the motion. The quiver plot of inertial compensation shows forces with a larger perpendicular component than seen in the other fields. This is another area of potential improvement for the compensator.

The controller may not be a perfect inertial compensator, but it has the desired effect across much of the workspace. In most cases it is able to assist in both the launching and braking phase of movements. This assistance amplifies the acceleration of the limb in response to muscle forces, effectively reducing its inertia.

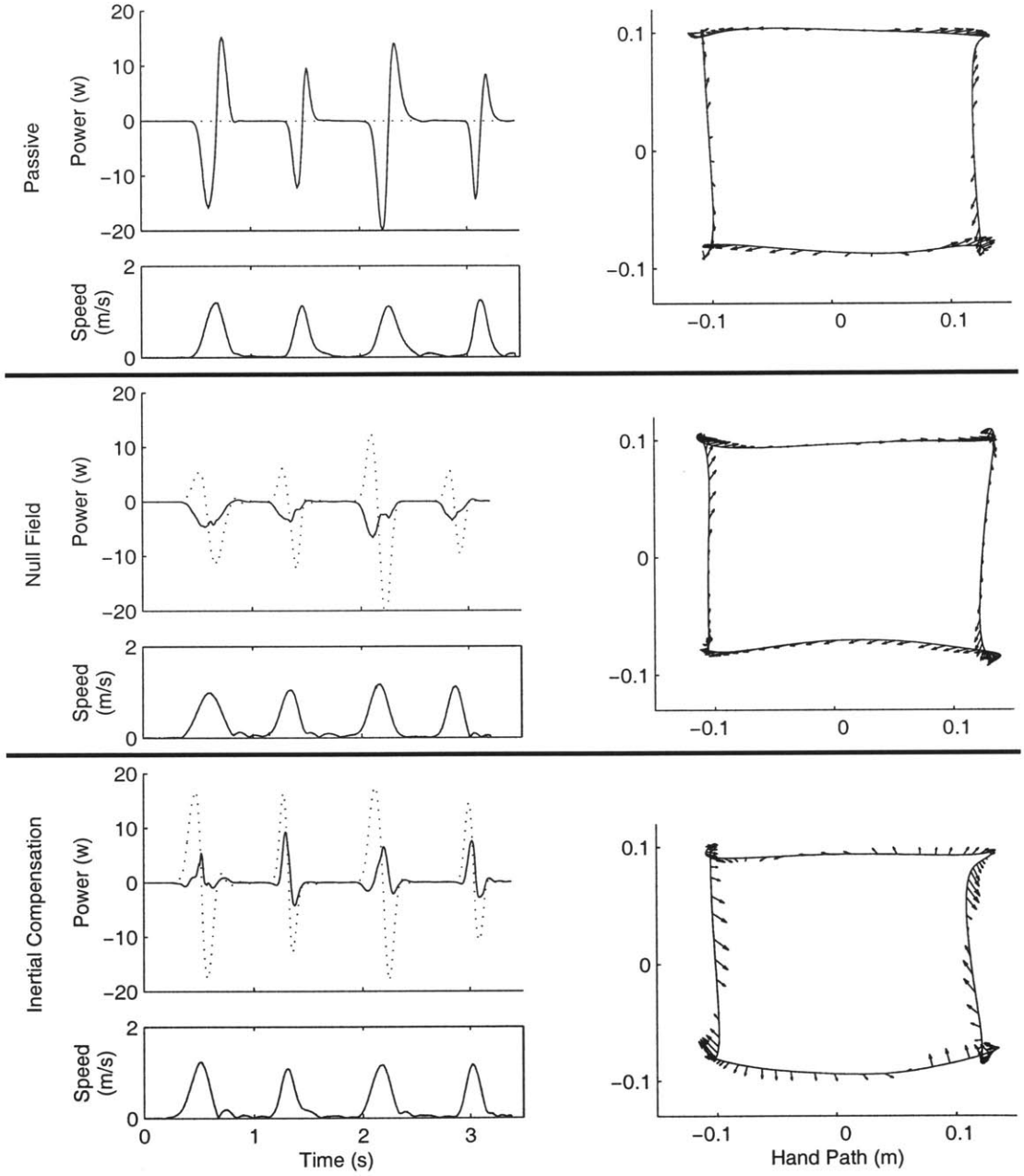

Figure 5-3: Power plots and quiver plots demonstrate the behavior of the manipulandum under three different controller: Passive, with motors applying zero force; Null field which minimizes the effect on the subject; and inertial compensation which attempts to reduce the effective mass of the subject's limb. Solid lines in the power plot depict power transferred to the hand, while dotted lines depict power transferred from the motors. Solid lines in the quiver plot show the hand path, and arrows indicate the force vector applied to the hand at that point along the path.

Chapter 6

Task Design

Previous testing has demonstrated that the compensator is capable of reducing the effective inertia of the limb, but this does not prove that it is effective in correcting the symptoms of ataxia. To demonstrate its capability in compensating for ataxia, a quantitative method for measuring the severity of ataxia deficits is required. Ideally, the task used for this measurement will be similar to tasks subjects encounter in the real world, and will be capable of elucidating many of the symptoms of ataxia.

A timed tracing task similar to the one used by Holmes [12] was used to measure the severity of ataxic errors. Tracing tests the ability of the subject to produce a desired hand path. Time limits force the subject to make movements that are fast enough to experience significant dynamic forces. Ataxic subjects tend to avoid high speed movements because these result in movement errors. The task imposes time limits to force subjects to make these errors so their severity can be judged.

Different dynamics become significant at different movement speeds. The effect of the compensator changes depending on the significance of inertial loading, so it is import to map out performance over a wide range of speeds. This is accomplished by running the subject through the same tracing task with a variety of time limits. Fitts has demonstrated that accuracy falls off logarithmically with speed [6]. We can document the performance of the compensator by measuring changes in this speed-accuracy curve.

6.1 Tracing Task

The tracing target is the 23 cm wide 18 cm high rectangle shown in figure 6-1. Subjects must trace this path in a counterclockwise direction. The rectangle is centered in front of the subject and the near edge is approximately 20 cm in front of the subject's chest. A small 1.3 cm diameter circle at the lower left corner of the rectangle serves as the target from which the subject must start. This task takes place in the horizontal plane, so targets that are closest to the subject will be referred to as near targets, and are displayed in the lower half of figure 6-1. Targets furthest from the subjects body will be referred to as far and will appear in the top half.

Larger targets, approximately 4 cm across, are placed over each of the corners of the rectangle. Subjects are encouraged to make smooth reaching movements between the centers of these targets rather than visually tracing the edges of the rectangle. These point-to-point movements tend to be faster and smoother than visually guided tracings and are less susceptible to intention tremor. This makes the movements more easily corrected by the inertial compensator.

Early versions of the task had the target path displayed on a computer screen with a cursor indicating the current location of handle. Some subjects had trouble quickly learning the mapping between hand position and cursor position on the monitor. one subject was observed occasionally making reaching movements away from his body when the task called for an inward movement as depicted by a downward turn in the target line on the computer screen. After noticing the upward movement of the cursor, the subject quickly altered his hand direction, and completed the task as expected. It is unclear whether this difficult was related to his cerebellar deficit or simple unfamiliarity with tasks that require the mapping of hand movements in the horizontal plane to cursor movements on a vertical computer screen.

To minimize complications from this visual coordinate transform, the final version of the task was setup with an LCD screen built into the table below the manipulandum as shown in figure 6-2. A small plastic rod was attached to the manipulandum handle to serve as a physical visual indicator in place of the cursor. This upgrade

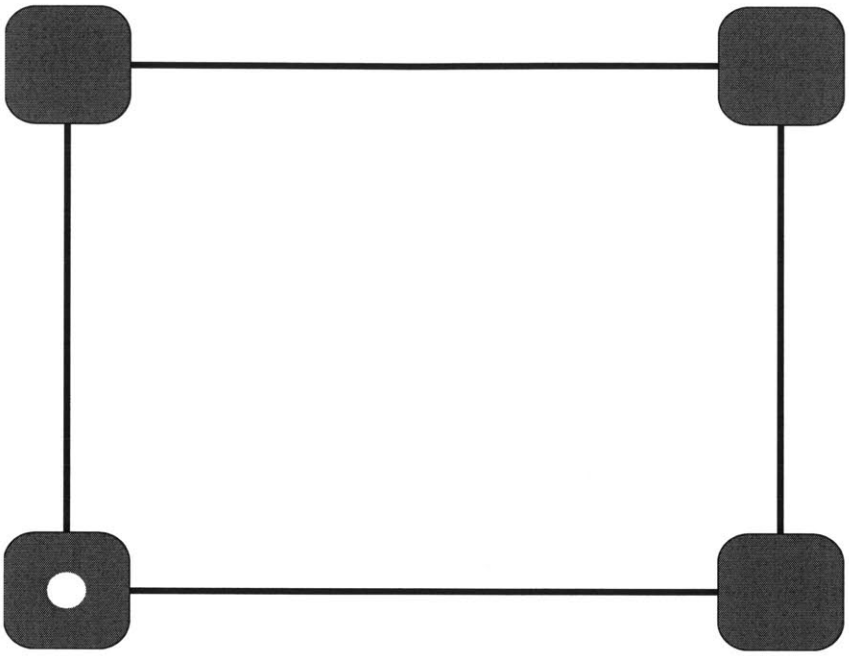

Figure 6-1: The goal path of the timed tracing task is a 23 cm wide, 18 cm high rectangle. 4 cm wide targets mark each of the four corners and a 1.3 cm diameter circle in the lower left corner marks the starting location. Subjects must trace the rectangle in a counterclockwise motion.

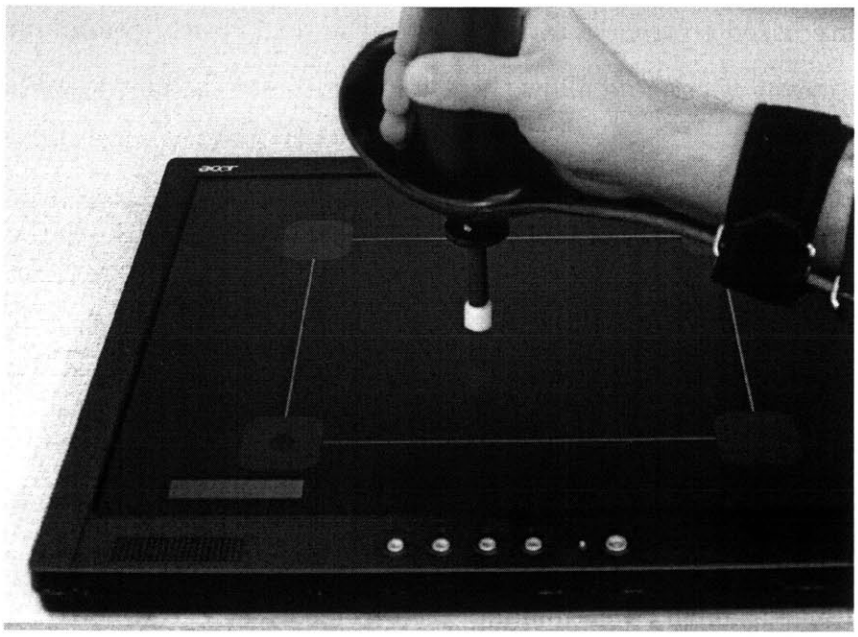

Figure 6-2: Visual targets are displayed on an LCD built into the table below the manipulandum. A visual indicator is affixed to the manipulandum handle and positioned just above the LCD.

allowed targets to be shown in the coordinate frame of the hand and eliminated any complications that may have arisen from the additional visual coordinate transform needed in the earlier version.

6.2 Accuracy Metric

To generate a speed-accuracy plot, a quantitative measure of the accuracy of any given tracing is required. The primary metric we made use of is the area of error of the movement. The area of error is the area enclosed between the desired hand path (in this case a rectangle) and the produced hand path. Figure 6-3 shows the area of error for a particular movement.

There are many other metrics that could be used, such as the time integral of the distance between the hand and the desired trajectory. Area of error has the advantage of being easily communicated to the subject. A simple plot of the enclosed area easily communicates to the subject the way in which they are being scored. This is advantageous because we cannot know exactly what the subject is optimizing for when they are asked to trace a target. Instead we can clearly communicate to them how we are scoring them, and allow them to optimize for the metric we have selected.

6.3 Area Algorithm

Finding a method for measuring the area between two arbitrary shapes can be difficult. It is not always obvious which parts of the observed and goal paths should be associated with each other. For example if the goal path crosses itself, and the hand path nears this intersection, then it may be unclear which leg of the goal path the hand path should be associated with. If incorrect parts of the path are associated with each other, then the area may be filled in incorrectly leading to an error in the area estimate.

These ambiguities can be cleared up by giving the tracing algorithm an internal state associated with where it believes the observed hand position should be if it were

perfectly tracking the goal path. This state can be pictured as a bead which slides along the goal path in a continuous manner. The bead is connected to the current hand position by a virtual spring. The area of error is then the area swept out by the spring. The introduction of this internal state can disambiguates many situations in which it is difficult to figure out which part of the desired path should be paired with a given part of the observed path.

The actual implementation differed slightly from the spring-bead model. The spring-bead model risks getting caught in local minima near sharp corners because it can only move the bead in directions that immediately shorten the spring. This problem is avoided by doing a broader search for the shortest spring distance along a section of the desired path. The extended search prevents the bead from being trapped in local minima while the limited search region prevents the bead from jumping ahead to ambiguous regions such as path crossings.

This algorithm is implemented in a discrete manner using triangles to fill the area between the paths. Each path is sampled with a roughly equal number of points. The algorithm iterates down the list of points in the observed path. With each point in the hand path it finds the nearest matching point on desired path by searching a range points around the last known near point. It then fill in triangles between the current and previous observed points and the list of points that lie along the desired path between the previous near point and the current near point. The output of this algorithm for a typical hand path is shown in figure 6-3.

6.4 Tracing Task Time Line

The time line of the tracing task is broken down into three phases: initiation, tracing, and feedback. During the initiation phase the subject must position the handle of the manipulandum over the small starting target and hold it here for one second. This insures consistent initial conditions for the tracing task. When the subject stays positioned over the target for one second, it will turn green indicating that it is now acceptable to begin the tracing task. The subject is now allowed to initiate the tracing

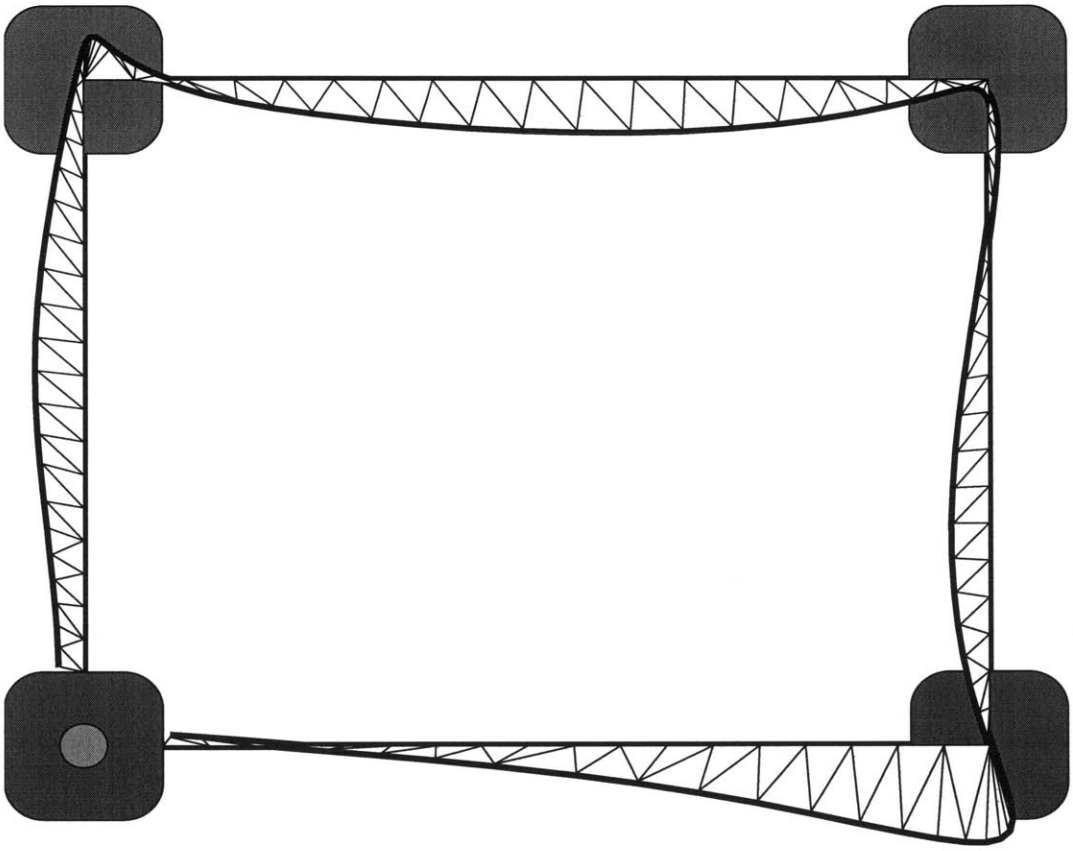

Figure 6-3: Triangles are used to determine the area of error between the goal rectangle and the produced hand path.

task whenever he is ready.

The tracing phase begins as soon as the subject leaves the area defined by the larger target in the near left corner of the rectangle. As soon as the tracing phase begins, an hourglass begins running down. The subject must trace the rectangle and return to the larger near left target before the hourglass runs out in order for the tracing to be considered successful. The task requires subjects to actively stop within this target and remain there for one second rather than simply pass through the target. The larger target is used to ensure that subjects will not have to overly restrict their movement speed to successfully stop at the goal.

Upon completion of the tracing phase, subjects are given feedback about their movement. Subjects are given an error message if their movement is too slow, or too inaccurate to be scored. If the movement is successful then the subject is given visual feedback and a score so that he can improve his performance as measured by the area of error metric.

Movements are considered too slow if the subject fails to return to the target area before the hourglass runs out. When this occurs a "Too slow" error message is presented on the screen. Movements that are too slow are still included in the results and analysis because they are valid tracing attempts. The error message simply serves to encourage subjects to move more quickly in the future.

Subjects are coached to trace the rectangle as accurately as possible in the allotted time. If they complete the task with excessive time on the clock then the operator encourages them to slow down and try to trace more accurately. If they do not complete the task in the allotted time then they are encouraged to worry less about accuracy and simply make sure they finish before the time limit. These rules make it possible to map out the subject's performance over a broad range of speeds.

In some movements the difference between observed hand path and the goal shape is so significant that the area of error metric cannot be used to judge the accuracy. In this case the subject is presented with a "Not a rectangle" error message. The bar for acceptable paths is set quite low. The only paths that are considered unacceptable are paths in which the virtual bead does not reach the end of the target path. In

practice this error condition occurs very infrequently, and generally happens when the subject is interrupted during the task and returns to the target without tracing the full rectangle. In the experiments presented in this thesis, this error condition only occurred once in 180 trials. These paths can not be accurately scored by the error metric so they are not included in the results.

If the tracing is considered successful, the subject is given feedback about his movement so he can optimize for the area of error. The subject is shown his hand path overlaid over the target hand path. An animation fills in the area between his path and the target path drawing his attention to the errors he made. The subject is also presented with a score corresponding to the area of error of the movement. This ensures that subjects understand the metric by which their accuracy is being judged so that they can take actions to optimize for it. Following completion of the feedback phase, the screen is redrawn and the task may begin again.

6.5 Experiment Organization

The tracing task is run many times throughout an experiment. Tracing tasks occur in blocks of six trials. The time limit is varied from block to block to map out the full speed vs. accuracy curve. Blocks of trials are assembled into four epochs. The forcefield is changed from epoch to epoch. In two epochs a null field is used as an estimate of performance when the machine is not present. In the other two epochs the inertial compensator is used. The performance can be compared from epoch to epoch to test the effectiveness of inertial compensation.

Within each epoch a wide variety of time limits are used. In the first block within each epoch, subjects are given infinite time to complete the tracing task. In the second block subjects are given ten seconds to complete the task, an easily achieved goal. In each subsequent block the test administrator lowers the time allotment until the subject is only rarely able to successfully complete the task within the allowed time. Testing over a wide range of speeds allows the subject's full speed accuracy curve to be mapped out.

This speed-accuracy curve is mapped out for each of the four epochs. In the first epoch, the null field is used as a way of approximating the subject's baseline performance in the absence of the machine. In the second epoch the inertial compensator is used to gauge its effectiveness at correcting the symptoms of ataxia. The third and fourth epochs are a repeat of the null and compensator fields. These epochs provide a way of disassociating changes in performance due to practice from changes due to differing forcefields. Figure 6-4 shows a time line for a typical experiment.

The structure of the experiment allows the subject time to become familiar with the forcefields. This is advantageous over a design in which the forcefield is changed from trial to trial, because the subject may need to alter his movement strategy to take full advantage of the compensator. The large number of consecutive trials in a consistent field helps facilitate this. The first trials of the experiment are in the null field because it is closest to the dynamics that subjects are used to. This means that the subject does not have to simultaneously learn the task and become acquainted with a novel force field. Within each epoch the time limit slowly progresses from long to short. This steadily increasing task difficulty also allows the subject time to practice with the forcefield before reaching more difficult levels.

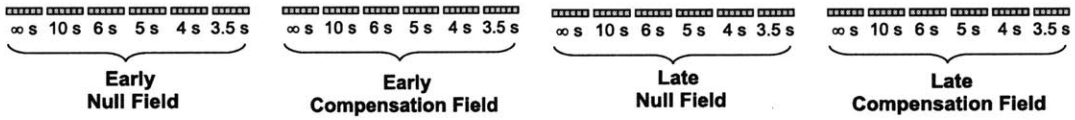

Figure 6-4: The time-line of the experiment is broken down into four epochs consisting of early and late versions of the compensator and null field. Each epoch is broken down into blocks of trials with different time limits.

Chapter 7

Human Experimental Results and Discussion

To date three subjects with cerebellar damage have participated in the experiment described in chapter 6. These subjects represent a several forms of cerebellar damage, and exhibit a wide range of symptoms. One subject exhibits both ataxic and endpoint tremor symptoms. Another subject has both cerebellar and cortical lesions, and demonstrates kinematic errors, but no tremor. The third subject has pure ataxic symptoms and shows no signs of tremor. The compensator demonstrated significant and consistent improvement for the subject with pure ataxic symptoms, but was unable to improve the performance of the other subjects with endpoint tremor or non-cerebellar lesions. This analysis will focus on the results of the one purely ataxic subject.

7.1 Ataxia Compensation

Subject P1 is a 30 year old male who suffers from a congenital defect that prevented his cerebellum from fully developing. The subject exhibits moderate levels of ataxia and shows no signs of endpoint tremor. The subject showed significant improvement in tracing performance with inertial compensation when compared against performance in the null field.

	Fast (2 s to 4 s)	Medium (4 s to 6 s)	Slow (6 s)
Early Null Field	105.31 ± 37.97	77.02 ± 13.63	84.34 ± 23.96
Early Compensation	85.97 ± 23.82	54.13 ± 17.02	51.65 ± 7.22
Late Null Field	111.75 ± 31.18	85.04 ± 21.38	61.13 ± 10.04
Late Compensation	76.77 ± 28.34	46.72 ± 6.50	47.69 ± 10.56
significance of difference			
between null and compensation	$p = 0.0033$	$p = 1.87 \times 10^{-11}$	*
between early and late	$p = 0.7173$	$p = 0.8547$	*

*not comparable due to differences in mean completion time

Table 7.1: Mean and standard deviation for area of error of the tracing task measured in cm^2 and sorted by epoch and time bin. Differences between null and compensated errors are significant while difference between early and late are insignificant.

Speed-accuracy plots were mapped out for subject P1 using the procedures described in chapter 6. Speed is measured by the time required to complete the tracing task and accuracy is judged by the area of error metric. Figure 7-1 shows speed-accuracy data for subject P1. Each data point corresponds to a single tracing movement. The data is sorted by forcefield epochs, with solid shapes representing movements in the compensation field and pluses and crosses representing movements in the null field. Pluses and circles represents trials that took place in the first half of the experiment, while diamonds and crosses represent movements in the second half.

The data is further divided into bins based on completion time. Completion times between 2 and 4 seconds are considered fast, 4 to 6 seconds are medium speed, and movements that take longer than 6 seconds are considered slow. Plots of the mean and standard deviation of the speed and accuracy data is shown in figure 7-1 and summarized in table 7.1.

At slow speeds we expect to see comparatively little error, and little difference between the accuracy of movements in the null field and when the compensator is active. This is because the limb does not experience large accelerations or large inertial forces, so the compensator has little effect. The compensated trials do exhibit lower mean area of error than uncompensated trials, but this difference is likely attributable to the lower mean completion time of the uncompensated trials. The small number of data points in this time bin makes further analysis difficult.

At slow speeds, the speed-accuracy plot approaches a minimum area of error

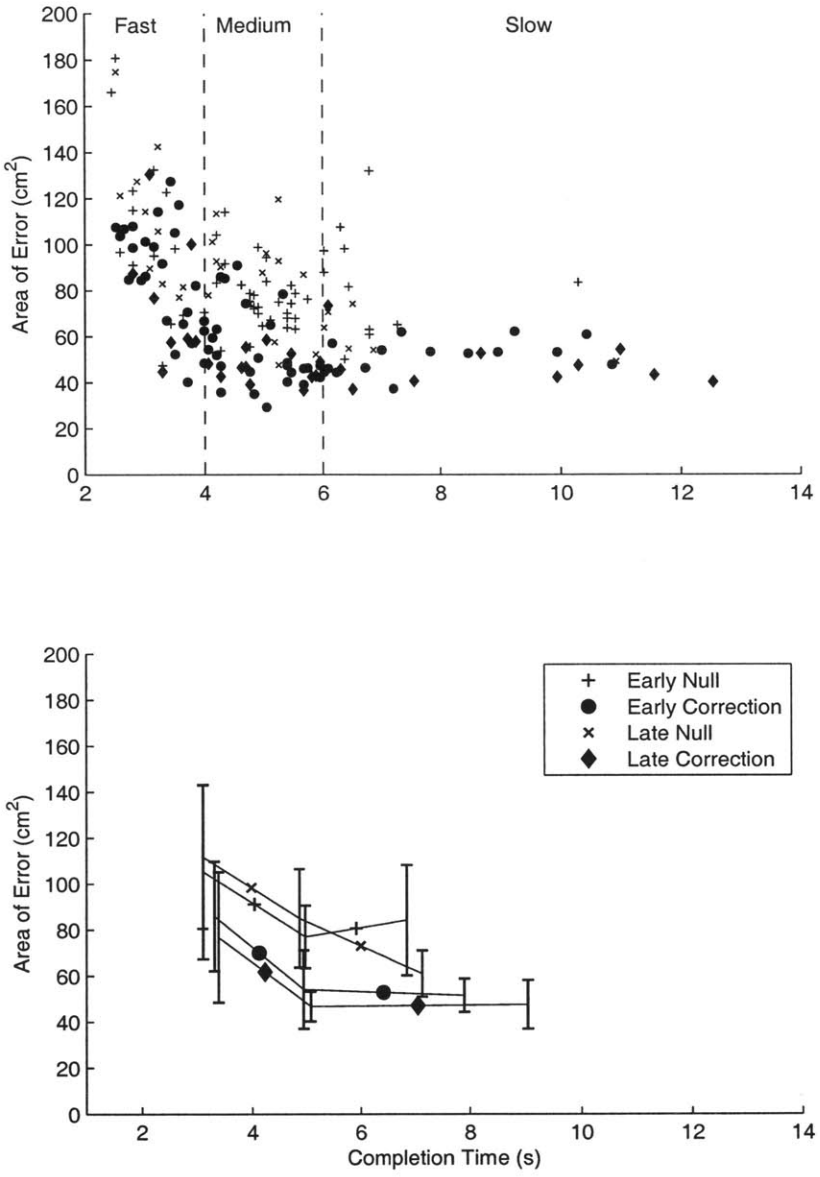

Figure 7-1: Speed vs. accuracy plots for the tracing task as measured by area of error and completion time. The data is divided into four epochs corresponding to early and late null field trials and early and late compensation. The mean and standard divination of area of error is shown for slow ($>$ 6 seconds completion time), medium (4s to 6s), and fast (2s to 4s) movements.

around 50 cm^2. This represents an average distance between the hand and goal paths of about 6mm. 6mm is approximately the same size as the radius of the visual indicator used to mark the manipulandum location over the target screen. The floor in the speed-accuracy plot is most likely due to the subject's ability to perceive alignment of the visual indicator and screen targets, rather than a limitation of the motor control system. Highly practiced, healthy subjects rarely score below 40 cm^2.

Medium speed movements show a dramatic effect from inertial compensation. In the null field, medium speed movements show the expected increase in area of error over slower movements. However, with the compensator active, medium speed movements have roughly the same tracing accuracy as slow speed movements. Null field movements have, on average, 65% more area of error than movements with inertial compensation. If we assume that the area of error in each field has a normal distribution, then we can use Welch's unpaired T-test to test the statistical significance of this improvement. The test yields a p-score of less than 10^{-10}, indicating that the odds are less than 1 in 10^{10} that this difference is the result of chance.

The difference in mean area of error cannot be attributed to a difference in mean completion time. There is a less than 1% difference in mean completion time between movements in the two fields. The improvement in performance is also not the result of a practice effect. The difference between mean area of error for early trials is within 1% of the mean error for late trials.

Movements that fall into the fast time bin also show improvements, though they are less statistically significant. The amount of area of error eliminated by the compensator is approximately equal to the amount reduced in the medium speed movements, but the significance, and percentage improvement, are much less because of increases in the overall error and the standard deviation of error. The compensated high speed movements have an accuracy on par with medium speed uncompensated movements. Uncompensated high speed movements have an average of 29% more area error then their compensated counterparts, with less than 1% odds that this difference is the result of chance. The improvement may also be slightly exaggerated due to a shift in mean completion time. Uncompensated movements within this time

A) High speed movements (< 2 second completion time)

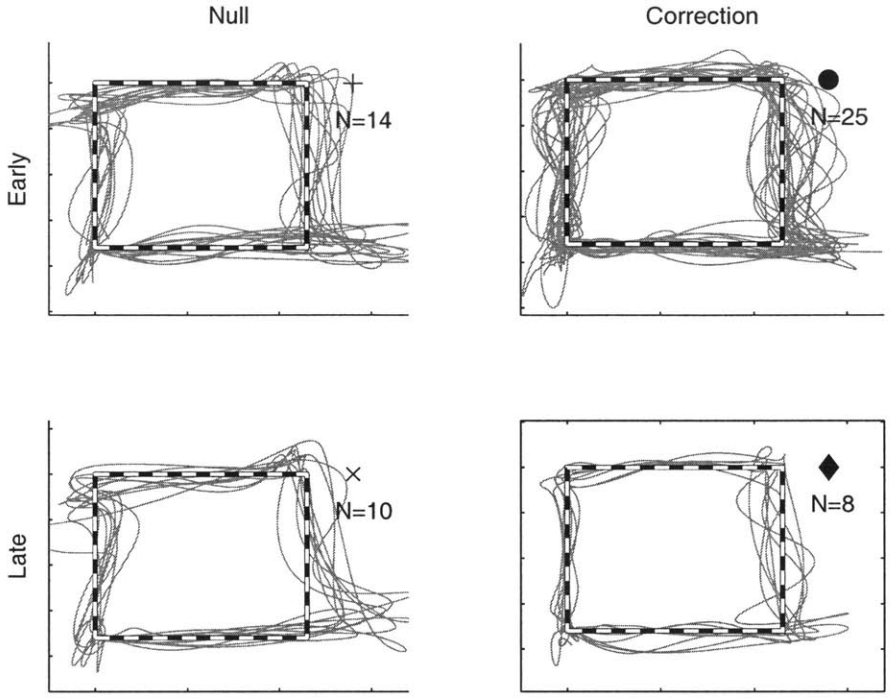

B) Medium speed movements (2 to 4 second completion time)

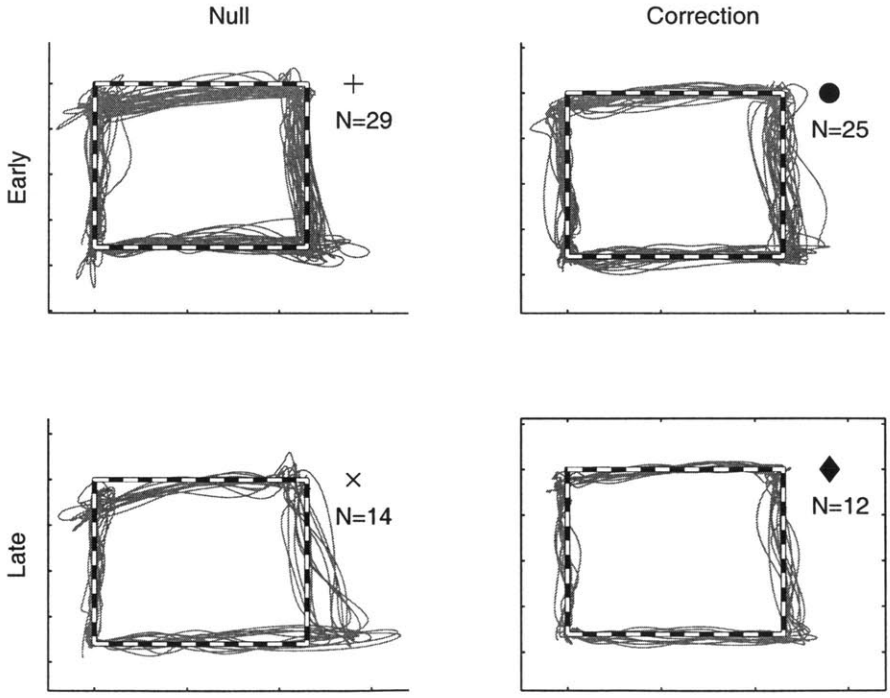

Figure 7-2: Hand paths for medium and high speed movements, for subject P1, during the timed tracing task.

block were, on average, 7% faster than compensated ones.

The reduction in performance at high speeds is not necessarily surprising. It is difficult for ataxic subjects to move at the speeds required to complete the task within the fast time bin. This results in the fast, poorly controlled movements shown in figure 7-2A. The equilibrium trajectory of these movements may not lie on the target rectangle, so the compensator may not be directing the movement in the exact direction of the target. The compensator's performance may also be reduced at these speeds due to the phase lag in the power transfer. Because of these limitations, the remainder of the analysis will focus on movements that fall in to the medium speed (4 to 6 second) time bin where the compensator is most effective.

7.2 Feature-Specific Improvements

The reduction in area of error can be attributed to several improvements in the shape of the hand path. These improvements can be seen in figure 7-2B, which shows plots of the hand paths within the medium speed time bin for each of the four forcefield epochs. These plots show that, among other improvements, the compensator was able to reduce the overshoot in the near right corner of the rectangle. It was also able to improve the tracking along the far edge of the rectangle. Overshoot and poor targeting in two-dimensions are common features of ataxic movements. We can analyze these improvements further through feature specific metrics.

The amount of overshoot in the near right corner can be measured by the peak excursion of the hand beyond the target rectangle. Figure 7-3 shows a detail of this overshoot. As the figure shows, the standard deviation of the overshoot is reduced by the compensator when compared with performance in the null field. In trials in the second half of the experiment, the compensator reduced the overshoot by more than 60%. This reduction was significant ($p < 10^{-3}$), but it is limited to the late trials. Large overshoot was less common in the early null trials. Some early null field trials showed much more overshoot than compensated trials, but the mean overshoot of these two groups did not have a statistically significant difference. The discrepancy

between mean overshoot values between the early and late null field trails may be an indication that an after effect of the compensation field is exaggerating overshoot in the late null field.

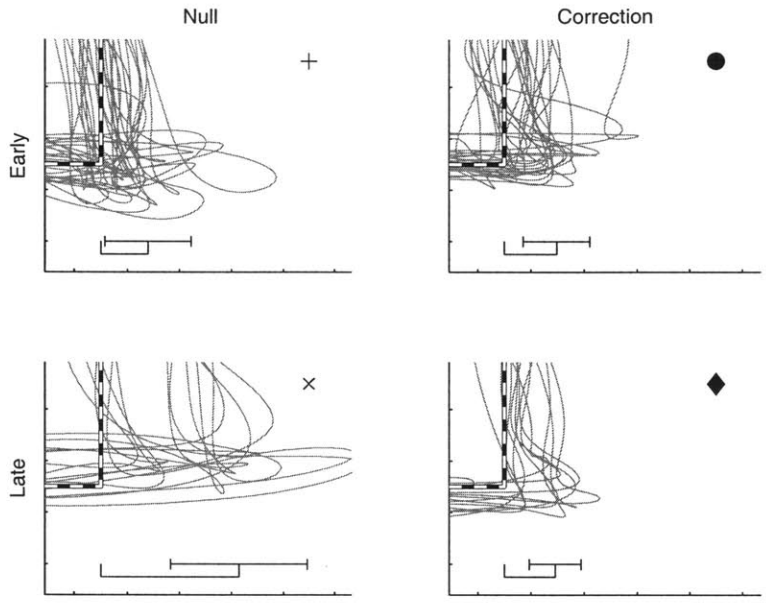

Figure 7-3: Detail, including mean and standard deviation, of the overshoot in the near right corner of the rectangle tracing task.

The compensator also improved the subjects ability to follow the far edge of the rectangle. Ataxic subjects often have an impaired ability to make straight, well aimed movements. These errors in aim can be quantified by the average angle between the hand path and desired path in this section of the work space. This is found by fitting a line to the selected part of the hand path and measuring the angle error. Figure 7-4 shows a detail of these errors.

This metric is not as sensitive as area of error to the effects of the compensator. This is presumably because area of error picks up other tracking errors in addition to the angle error. The angle error metric shows that in late movements, the compensator is able to reduce the angle error by more than 40%, though there are 10% odds that this improvement is the result of chance. In early movements the angle error is reduced by 20%, and the odds that this happened by chance are less than 15%.

These results, particularly for medium speed movements, demonstrate that inertial compensation can significantly reduce kinematic errors in ataxic patients. The compensator significantly improves the patient's deficit in moderate-speed tracing accuracy. This improvement is at least partly the result of reductions in overshoot, a common result of cerebellar damage, as well as improvements in two-dimensional targeting, another common deficit.

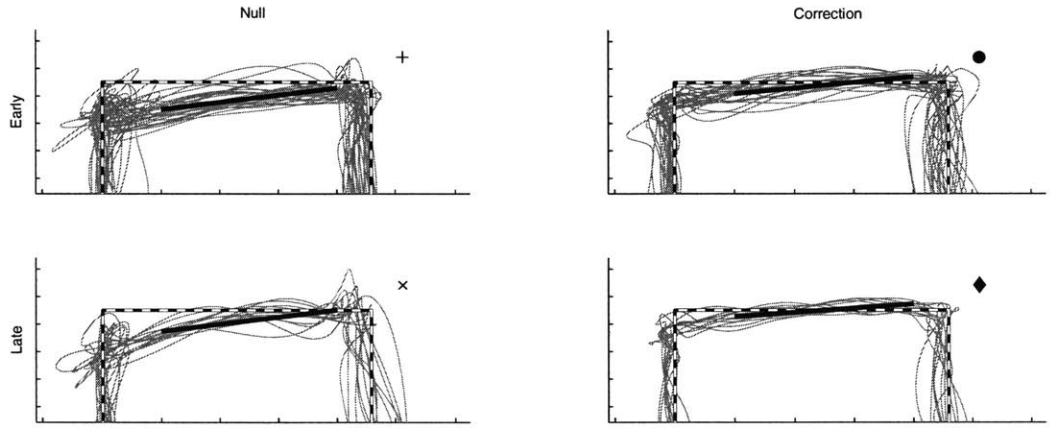

Figure 7-4: Detail, including fit line, of the tracking error of the far edge of rectangle tracing task

7.3 Effects on Non-purely Ataxic Subjects

In addition to the purely ataxic subject, two other subjects participated in the experiment. Subject P2 is a 60 year old female with cerebellar damage resulting from an as yet undetermined, possibly auto-immune mechanism. The subject exhibited moderate to severe levels of ataxia as well as moderate to severe levels of endpoint tremor. Attempting to perform the tracing task resulted in significant tremor, even in the absence of inertial compensation. The inertial compensator further exaggerated this problem by amplifying acceleration and causing larger oscillations. In uncompensated movements, the limb's inertia presumably impedes these oscillations, so reducing the effective inertia leads to greater tremor. The resulting tremor prevented the subject from being able to complete the tracing task.

Subject P3 is a 40 year old female whose has both cerebellar and cortical damage as the result of physical trauma experienced during an automobile accident. The patient does not show signs of significant tremor, but does show errors in voluntary movement. These errors may be the result of cerebellar damage, though they exhibit features that are not traditionally associated with ataxia. For example, the subject shows steady state error when attempting to reach for targets in specific parts of the workspace. This can not be explained by failure of dynamics compensation and may be the result of cortical lesions. The compensator is designed for errors in dynamic compensation and was therefore unable to affect these errors. The subject was able to complete the experiment but showed no signs of a significant difference in performance in the null field and inertial compensation fields.

Chapter 8

General Discussion and Conclusions

Many interesting discoveries have been made in the area of motor neuroscience, but so far there have been relatively few practical applications of this knowledge. This thesis has shown that models of the human motor control system can be useful in both understanding the deficits that result from damage to the nervous system, and in developing engineering-based interventions to compensate for these impairments.

We have demonstrated that if the motor system fails to compensate for the dynamics of the limb, then the resulting kinematics are consistent with many of the errors observed in ataxia. For high-speed planar reaching movements these dynamics are dominated by inertia. We have confirmed that inaccuracies in the reaching movements of an individual with cerebellar ataxia, are at least partly due to these dynamics, by showing that robotic cancellation of inertial effects significantly improves tracing accuracy. If this result can be reproduced in a larger population then it will have significant implications in the areas of motor neuroscience and medical treatment of this disorder.

8.1 Possible Scientific Implications

Several researchers have demonstrated that the cerebellum plays a role in compensating for external dynamics when they are coupled to the limb [13, 27, 20]. Topka [29], Bastian [2], and many others have argued that the cerebellum also plays a critical role in managing body dynamics, but this has not been experimentally tested until now. The research presented in this thesis provides a technique for confirming that the cerebellum compensates for limb dynamics. This is done by demonstrating that, at least some, of the movement errors that occur when the cerebellum is damaged, are the result of failure to compensate for limb dynamics. The source of these errors was confirmed by showing that robotically canceling some of the limb dynamics results in a significant reduction in ataxic errors.

Understanding the cause of movement errors in subjects with cerebellar ataxia gives insight into the function of the cerebellum in healthy subjects. Overshoot of targets is one example of a common symptom of cerebellar damage. In healthy subjects, it is believed that the cerebellum helps compensate for the limb inertia by sending signals to the muscles that help bring the limb to a stop. In subjects with cerebellar ataxia, this dynamic compensation appears to be at least partly impaired, resulting in the overshoot that is commonly observed in ataxia. This research has provided preliminary experimental evidence that supports the idea that overshoot is related to limb inertia by showing in the tracing task, large overshoot was less likely to occur when the effective inertia of the limb was reduced.

Another example of a common symptom of ataxia is the swerving and poor targeting that is observed in two dimensions. This error is consistent with failing to compensate for the anisotropies of the limb inertia. When an ataxic subject initiates a movement, the launch tends to veer towards the direction of minimal inertia rather than being targeted directly at the goal. An example is the error in tracking observed in subjects near the far edge of the rectangle in the tracing task. Near the far right corner of the rectangle, the anisotropic inertia makes acceleration down and inward easer than accelerating along the far edge. When performing the tracing task in the

null field the ataxic subject was observed making significant deviations inward. When the compensator was active, and the limb anisotropy reduced, the subject was able to significantly improve his tracking of the far edge of the target rectangle.

Overshoot and poor targeting, along with other kinematic errors, make up the general "clumsy" appearance of ataxic movements. The area of error metric is able to capture all of these effects by measuring the overall accuracy of reaching movements. This metric indicated that, for medium speed movements, the compensator was able to reduce kinematic errors by 40% when the subject's limb inertia was reduced by roughly 40% in parts of the workspace. This is a strong demonstration that the dynamics that the compensator cancels are largely responsible for the errors observed in this subject's movement.

It is dangerous to make any conclusions based on data from a single subject. There is always a chance that the subject is not an accurate representative of the overall ataxic population. These experiments need to be reproduced in a larger population for these results to be made conclusive. The experiment is, however, a demonstration that in at least one subject, robotic compensation of cerebellar ataxia is possible.

The theory that ataxic errors are the result of a failure of dynamic compensation is quite useful. It provides a unified explanation for the underlying cause of many of the observed symptoms of ataxia. It supports the theory that the cerebellum acts as a dynamic compensator, and is consistent with functional models of the cerebellum based on anatomical details, such as the feedback error learning model and the RIPID model. Most importantly from a medical standpoint, the model is capable of predicting the errors that result from cerebellar damage, and can therefore be used as the basis for a mechatronic compensation system.

8.2 Engineering Contribution: Compensator Design

Developing a stable inertial compensation system to correct for ataxia is a significant engineering challenge. The dynamics of the limb and motor control system must be modeled, along with the dynamics of the robotic system used to implement the compensator. Dynamics that are not typically included in these models, such as internal resonance modes, must be added to insure stability of the closed loop system.

This thesis both developed a design for an inertial compensator, and demonstrated its effectiveness in several ways. First, a mock arm was constructed for testing purposes. The mock arm had known, consistent dynamics similar to the average dynamics of the human arm. The similarity was confirmed by experimentally mapping out the frequency response of both systems. The compensator was tested by measuring its effect on the step response of the mock arm. The compensator succeeded in increasing the natural frequency and damping ratio of the system and showed that 70% of the mock arm's inertia could be effectively eliminated. Plots of the power transfer into the mock arm were also consistent with this effective mass reduction.

A two-dimensional compensator for use with human subjects was also designed. Power plots were used to show that the behavior of the controller was largely consistent with the behavior of an inertial compensator across much of the workspace. The compensator was then applied to an ataxic subject during a timed tracing task. The compensator was able to reduce the severity of some features of ataxia by as much as 40% by canceling roughly 40% of some the subject's limb dynamics in parts of the workspace. This demonstrates that ataxia compensation is possible and that the proposed model of the underlying derangement is probably accurate.

8.3 Medical Applications

This experiment is the first demonstration of mechatronic treatment of cerebellar ataxia. There are currently over 15,000 individuals suffering from cerebellar ataxia

in the United States, and for the vast majority of these, there are no viable treatment options. The compensation system studied here has demonstrated that dynamic correction of ataxic errors is possible. The compensator appears to address the fundamental mechanical control deficit in ataxia, which means there is a potential for treating a wide range cerebellar afflictions with a single orthotic device.

This experiment potentially brings the treatment of cerebellar ataxia into the engineering domain. It has demonstrated that models of neural control systems offer explanations for the underlying causes of ataxia and suggest methods for compensation. Careful modeling, identification, and analysis resulted in a compensator design that significantly improved the movement accuracy of a subject with ataxia. Refinement of this compensator will likely yield further improvements. There is still much work to be done before this is a viable treatment option, but the experiment serves as a demonstration that, in at least some cases, this form of correction is possible.

Chapter 9

Future work

There are several extensions to this research that will expand its significance. In the short term, the experiment needs to be performed on a larger population so that the generality of the work described here can be confirmed. Also, there are a number of simple changes that should be made to the controller that will likely improve its performance and make the observed effect more dramatic. In the long term, there are number of important changes needed to improve the practicality of the compensator as a medical treatment option.

9.1 Further Experimentation

The most important future work involves running the current experiment with a larger population. Little can be concluded from experimental results from a single individual. We must identify more subjects with significant ataxia and minimal propensity for endpoint tremor so that they can successfully complete this experiment. Demonstrating that the observed effect can be generalized beyond one individual will be an important confirmation of the theory presented here.

The experiment itself, could also be improved in several ways. For example an improved null field would ensure that no additional dynamics are introduced into the baseline estimate of the subject's performance. A nearly ideal null field can be implemented by replacing the manipulandum with an optical sensor, or similar

tracking device that does not have appreciable mechanical dynamics. This sensor could be coupled to a lightweight arm brace, suspended from the ceiling by wire to ensure the planar nature of the task. The disadvantage to this approach is that it becomes obvious to the subject which movements are made in the null field. One approach may be to use manipulandum generated null fields for the experiment, then later confirm that these movements are typical of null field performance by comparing with optically measured movements.

Another improvement may be to reduce the range of target completion times for the tracing task. Currently subjects make very few movements at any given speed. This is necessary to map out the behavior over a wide range of speeds, but makes observing practice and adaptation difficult. Ataxic subjects have an impaired ability to adapt to forcefields, but this impairment may not be complete. Running the task many times at a given speed will allows any adaptation to the compensator to be observed. It also reduces the danger that the observed effects result from performance transients or adaptation aftereffects. This danger was highlighted in chapter 7 by the increased overshoot that was observed in the late null field but not the early null field. Other corrected errors were observed in both null fields so this effect is incapable of explaining all of the observed improvements, though it may contribute to some of the changes.

The accuracy of this experiment is limited by the accuracy of the inertial compensator. Subject P1 participated in this experiment twice during the development of the compensator. Improvement in the mass reduction ability of the compensator were met with improved differentiation of performance in null and compensation fields. The performance of the current version leaves room for significant improvement, as can be seen in the power and quiver plots presented in chapter 5. Changes to the design that maximize its inertial compensation while minimizing the introduction of other dynamics will improve the quality of this experiment and likely increase the impact on ataxia.

9.2 Improvements to the Current Compensator

A number of simplifying assumptions were made during the design of the inertial compensator. These assumptions simplified the implementation of the compensator, but also limited its performance. Eliminating these simplifying assumptions leads to a design with improved ability to compensate for limb inertia, and presumably will lead to greater reductions the severity of ataxia.

One of the major performance-limiting factors in the current implementation is the constant coefficient mass reduction matrix. The reduction matrix cannot track the configuration dependent limb inertia, so that there are significant deviations in magnitude, orientation and aspect ratio between the limb inertia and the reduction inertia ellipses. This prevents the limb inertia isotropy from being improved throughout the workspace. The mismatch between these ellipses also limits the total amount of mass reduction that is possible. The system must be stable throughout the workspace, so the reduction matrix magnitude is limited to a conservative value that is compatible with all configurations.

These limitations could be eliminated by making the mass reduction matrix a function of a two-dimensional, configuration dependent arm model. This model would require an additional calibration phase in the experiment where subject-specific constants can be identified. The controller should also be extended to include the Coriolis and centripetal terms associated with the configuration dependence of limb and manipulandum masses. The addition of an angle sensor between the manipulandum handle and the arm support would also improve the estimate of the subject's arm configuration and minimize errors due to trunk and shoulder blade movement.

The isotropic constant coefficient nature of the lead-lag compensator also requires that it be highly conservative. Further mapping of the internal resonance modes of the system will allow for more aggressive filters in some directions and some locations within the workspace. Pushing the poles of the filter to higher frequency will increase the bandwidth over which inertial compensation is active and improve the performance of the compensator.

9.3 Practical Medical Applications: Addressing Endpoint Tremor

A major limitation of the current compensation system is its incompatibility with endpoint tremor. It is very common for tremor to appear along side ataxia in subjects with cerebellar damage. The compensation system would be applicable to a much larger population if this incompatibility can be addressed.

Developing a compensation system for endpoint tremor is difficult. The frequency band of the tremor overlap significantly with the frequency band of intentional movement, making discrimination difficult. At the initiation of movement, the kinematics of the limb offer few clues as to whether the movement is an intentional movement that should be assisted or an unintentional tremor that the controller should retard.

The overlapping frequency bands prevent the controller from getting enough information from the kinematics to determine the proper response. The controller needs access to additional information to determine if a movement is intentional. The simplest way to obtain this information is to provide the subject with a method for communicating his intent to the controller. For example, a grip sensor could be added to the manipulandum, and the subject could be instructed to squeeze the handle when they wish to stay still. The controller could then use this information to determine which movements are intentional and should be assisted and which are tremor related and should be retarded.

This is a less elegant system than the pure inertial compensator because the subject must learn to communicate additional information to the machine. A more attractive solution might attempt to address the underlying dynamics that cause the tremor. If the tremor results from poorly managed loop gains in the presence of significant transmission delays, then canceling these dynamics will be very difficult without access to the internal signals within the nervous system. Researchers are currently advancing our abilities to access and interpret such signals [4]. Having access to these signals will open up many more possibilities for compensation of motor control deficits.

9.4 Portability and usefulness outside of the lab

This research demonstrates that mechatronic compensation of ataxic impairments is possible, but it did so by coupling the subject to a heavy, non-portable manipulandum. Moving the compensation system out of the laboratory requires developing a lightweight robust system that can travel with the subject. Researchers have had some success developing exoskeleton systems for assisting human movement [16, 28, 18] but the high bandwidth required by the inertial compensator and the high power density required by the portable system make this a very challenging problem.

An interesting alternative to external actuators may be to use the subjects' own muscles to alter their movements. Most ataxic subjects have fully functional muscles that could produce the desired movement if they were sent the correct signal. It may be possible to develop a compensation system that senses the subject's movement, determines the additional signals to be sent to the muscles, and introduces these signals through functional electrical stimulation. This approach is quite attractive because it eliminates the need for external actuators and associated power sources.

One of greatest dangers ataxic patients are exposed to are falls due to tripping or poor foot placement. These gait errors are likely due to improper dynamic compensation of the forces experienced by legs. The first practical application of ataxia compensation may be a muscle stimulator that tracks the state of the legs and manipulates the gait to help prevent unintended impacts between the foot and ground.

There are many possibilities for other orthotic devices that can interact with the human motor control system to improve the lives of patients with motor deficits. Developing models of the motor system, and of motor control impairments, deepens our understanding of these deficits and brings the possibility of treatment into the engineering domain. This research demonstrates that cerebellar ataxia is one such impairment that can in at least some cases be corrected with artificial compensation systems. The possibilities for further compensation of motor impairments will only grow as our understanding of the motor system increases and our ability to design machines that interact with it improves.

Bibliography

[1] J. Babinski. Asynergie et inertie cerebelleuse. *Revista de Neurologia*, 14:685–686, 1906.

[2] A. Bastian, T. Martin, J. Keating, and W. Thach. Cerebellar ataxia: abnormal control of interaction torques across multiple joints. *Journal of Neurophysiology*, 76:492–509, 1996.

[3] E Bizzi, N Hogan, F Mussa-Ivaldi, and S Giszter. Does the nervous system use equilibrium-point control to guide single and multiple joint movements? *Behavioral and Brain Sciences*, 15(4):603–613, 1992.

[4] L. Hochberg et al. Neuronal ensemble control of prosthetic devices by a human with tetraplegia. *Nature*, 442:164–171, 2006.

[5] A. Feldman. Once more on the equilibrium-point hypothesis (lambda model) for motor control. *Journal of Motor Behavior*, 18(1):17–54, 1986.

[6] P. Fitts. Cognitive aspects of information processing. 3. set for speed versus accuracy. *Journal of Experimental Psychology*, 1966.

[7] T. Flash and N. Hogan. The coordination of arm movements: an experimentally confirmed mathematical model. *Journal of Neuroscience*, 5:1688–1703, 1985.

[8] B. Gillespie and M. Cutkosky. Stable user-specific haptic rendering of the virtual wall. *Proc. ASME Int"l Mechanical Eng. Conf. and Exposition*, 58:397–406, 1996.

[9] R. Gurram, S. Rakheja, and J. Brammer. Driving-point mechanical impedance of the human hand-arm system: Synthesis and model development. *Journal of Sound and Vibration*, 180(3):437–458, 1995.

[10] R. Hewer, R. Cooper, and M. Morgan M. An investigation into the value of treating intention tremor by weighting the affected limb. *Brain*, 95(3):579–590, 1972.

[11] N Hogan. An organizing principle for a class of voluntary movements. *Journal of Neuroscience*, 4:2745–2754, 1984.

[12] G. Holmes. The cerebellum of man. *Brain*, 62(1):1–30, 1939.

[13] J. Hore and T. Vilis. Loss of set in muscle responses to limb perturbations during cerebellar dysfunction. *Journal of Neurophysiology*, 51(6):1137–1148, 1984.

[14] S. Jo and S. Massaquoi. A model of cerebellum stabilized and scheduled hybrid long-loop control of upright balance. *Biological Cybernetics*, 91(3):188–202, 2004.

[15] E. Kandel, J. Schwartz, and M. Jessell. *Principles of Neural Science.* McGraw-Hill, 2000.

[16] H. Kawamoto and Y. Sankai. Comfortable power assist control method for walking aid by hal-3. *Systems, Man and Cybernetics, 2002 IEEE International Conference on*, 4:6, 2002.

[17] M. Kawato and H. Gomi. A computational model of four regions of the cerebellum based on feedback-error learning. *Biological Cybernetics*, 68(2), 1992.

[18] H. Kazerooni. Human-robot interaction via the transfer of power and information signals. *Man and Cybernetics, IEEE Transactions on*, 20(2):450–463, 1990.

[19] R. Lechtenburg. *Handbook of Cerebellar Diseases.* New York: Marcel Dekker, 1993.

[20] M. Manto, E. Godaux, and J. Jacquy. Cerebellar hypermetria is larger when the inertial load is artificially increased. *Annals of Neurology*, 35(1):45–52, 1994.

[21] M. Manto and M. Pandolfo. *The cerebellum and its disorders.* Cambridge University Press, 2002.

[22] T. Martin, J. Keating, H. Goodkin, A. Bastian, and W. Thach. Throwing while looking through prisms: Focal olivocerebellar lesions impair adaptation. *Brain*, 119(4):1183–1198, 1996.

[23] M. Maschke, C. Gomez, T. Ebner, and J. Konczak. Hereditary cerebellar ataxia progressively impairs force adaptation during goal-directed arm movements. *Journal of Neurophysiology*, 91:230–238, 2004.

[24] S. Massaquoi and M. Hallett. Kinematics of initiating a two-joint arm movement in patients with cerebellar ataxia. *Canadian Journal of Neurological Sciences*, 23(1):3–14, 1996.

[25] J. Michaelis. Mechanical methods of controlling ataxia. *Baillieres Clinical Neurology*, 2(1):121–139, 1993.

[26] N. Schweighofer, M. Arbib, and M. Kawato. Role of the cerebellum in reaching movements in humans. i. distributed inverse dynamics control. *European Journal of Neuroscience*, 10(1):86–94, 1998.

[27] M. Smith and R. Shadmehr. Intact ability to learn internal models of arm dynamics in huntington's disease but not cerebellar degeneration. *Journal of Neurophysiology*, 93:2809–2821, 2005.

[28] J. Stein, K. Narendran, J. McBean, K. Krebs, and R. Hughes. Electromyography-controlled exoskeletal upper-limb-powered orthosis for exercise training after stroke. *American Journal of Physical Medicine and Rehabilitation*, 86(4):255–261, 2007.

[29] H. Topka, J. Konczak, K. Schneider, A. Boose, and J. Dichgans. Multijoint arm movements in cerebellar ataxia: abnormal control of movement dynamics. *Experimental Brain Research*, 119(4):493–503, 1998.